Recalculated probability of $M \geq 7$ earthquakes beneath the Sea of Marmara, Turkey

Tom Parsons

U.S. Geological Survey, Menlo Park, California, USA

Received 1 July 2003; revised 23 December 2003; accepted 5 February 2004; published 22 May 2004.

[1] New earthquake probability calculations are made for the Sea of Marmara region and the city of Istanbul, providing a revised forecast and an evaluation of time-dependent interaction techniques. Calculations incorporate newly obtained bathymetric images of the North Anatolian fault beneath the Sea of Marmara [*Le Pichon et al.*, 2001; *Armijo et al.*, 2002]. Newly interpreted fault segmentation enables an improved regional A.D. 1500–2000 earthquake catalog and interevent model, which form the basis for time-dependent probability estimates. Calculations presented here also employ detailed models of coseismic and postseismic slip associated with the 17 August 1999 M = 7.4 Izmit earthquake to investigate effects of stress transfer on seismic hazard. Probability changes caused by the 1999 shock depend on Marmara Sea fault-stressing rates, which are calculated with a new finite element model. The combined 2004–2034 regional Poisson probability of $M \geq 7$ earthquakes is ~38%, the regional time-dependent probability is 44 ± 18%, and incorporation of stress transfer raises it to 53 ± 18%. The most important effect of adding time dependence and stress transfer to the calculations is an increase in the 30 year probability of a $M \geq 7$ earthquake affecting Istanbul. The 30 year Poisson probability at Istanbul is 21%, and the addition of time dependence and stress transfer raises it to 41 ± 14%. The ranges given on probability values are sensitivities of the calculations to input parameters determined by Monte Carlo analysis; 1000 calculations are made using parameters drawn at random from distributions. Sensitivities are large relative to mean probability values and enhancements caused by stress transfer, reflecting a poor understanding of large-earthquake aperiodicity. *INDEX TERMS:* 7223 Seismology: Seismic hazard assessment and prediction; 7230 Seismology: Seismicity and seismotectonics; 8150 Tectonophysics: Plate boundary—general (3040); *KEYWORDS:* earthquake probability, Sea of Marmara, seismic hazard, Turkey, stress interaction, North Anatolian fault

Citation: Parsons, T. (2004), Recalculated probability of $M \geq 7$ earthquakes beneath the Sea of Marmara, Turkey, *J. Geophys. Res.*, *109*, B05304, doi:10.1029/2003JB002667.

1. Introduction

[2] The North Anatolian fault cuts across northern Turkey for more than 1500 km, accommodating ~25 mm/yr of right-lateral motion between Anatolia and the Eurasian plate [e.g., *McClusky et al.*, 2000]. This fault has generated 13 $M \geq 6.7$ earthquakes in the 20th century, often with tragic results. This paper focuses on the hazard posed by the western North Anatolian fault, where about 25% of Turkey's people (~16 million) live, and where the fault plunges beneath the Sea of Marmara (Figure 1). Since 1 A.D., ~55 $M \geq 6.7$ earthquakes have shaken the Marmara region (Figure 1), many causing extreme damage [*Ambraseys*, 2002].

[3] Much scientific effort is devoted to the Marmara Sea region because of the long record of damage to large cities such as Istanbul (population ~9.5 million in 2003), and because in this area, the North Anatolian fault is submerged beneath the Marmara Sea, causing major uncertainties as to its location, continuity, and earthquake recurrence. Additional complications arise because the plate boundary changes from mostly right-lateral transform in the east into a transtensional system that has opened deep basins beneath the Sea of Marmara [*Armijo et al.*, 1999]. Thus there is a possibility of damaging earthquakes occurring both on normal and strike-slip faults.

[4] The purpose of this paper is to incorporate recent scientific breakthroughs into a new earthquake probability analysis of the northern Marmara Sea region, and to quantify their impact. New high-resolution images of the Marmara seafloor enable detailed fault mapping for the first time [*Le Pichon et al.*, 2001; *Armijo et al.*, 2002], which in turn affects assigned locations and recurrence of historic earthquakes (Figure 2). A new regional earthquake attenuation relation [*Ambraseys*, 2002] enables better calculation of historic earthquake magnitudes from intensity values. Preliminary calculations of stress change caused by the 1999 M = 7.4 Izmit earthquake on Marmara Sea faults showed likely impact on their rupture potential [e.g., *Hubert-Ferrari et al.*, 2000; *Parsons et al.*, 2000]. Intensive

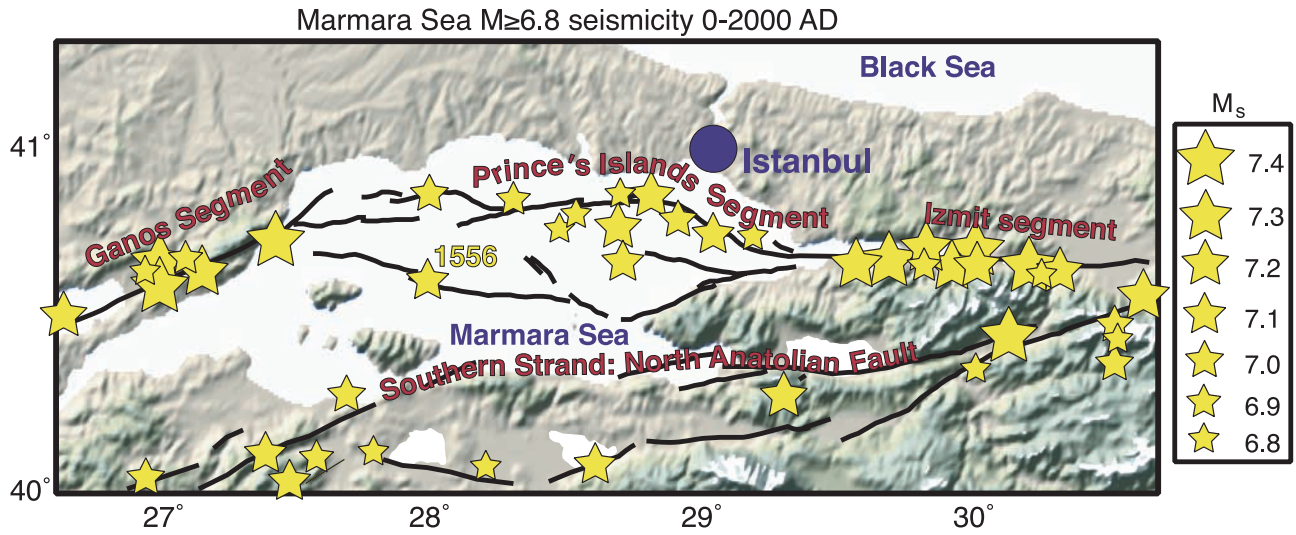

Figure 1. Segments of the North Anatolian fault beneath the Sea of Marmara [*Armijo et al.*, 2002] and locations of $M_s \geq 6.6$ earthquakes (A.D. 1–1999) as located by *Ambraseys* [2002].

study of the Izmit earthquake has resulted in more detailed models for coseismic and postseismic slip [*Reilinger et al.*, 2000; *Bouchon et al.*, 2002; *Bürgmann et al.*, 2002; *De Louis et al.*, 2002; *Li et al.*, 2002], which improve stress change calculations on Marmara Sea faults, as do the improved fault locations [*Le Pichon et al.*, 2001; *Armijo et al.*, 2002].

[5] To recalculate the probability of earthquakes beneath the Sea of Marmara, I first develop a new earthquake catalog for the period between A.D. 1500 and 2000 using new fault maps and the technique of *Bakun and Wentworth* [1997] modified with the regional attenuation relation of *Ambraseys* [2002]. This catalog enables new interevent and elapsed time values for use in probability calculations. Next, new coseismic and postseismic models of Izmit earthquake slip are used to calculate stress changes on the new Marmara Sea fault model; resulting earthquake advances and delays are calculated using these stress change values and new tectonic loading rates determined from finite element modeling of the Sea of Marmara segment of the North Anatolian fault. Results from these modeling exercises are used to make up-to-date probability calculations for the Marmara Sea that fully incorporate coseismic and postseismic stress interactions from the 1999 Izmit earthquake.

2. $M \geq 7$ Earthquake Catalog: A.D. 1500–2000

[6] In the period between A.D. 1500 and 2000, nine $M \geq 7$ earthquakes occurred beneath, or partly beneath, the Sea of Marmara (Figure 3), a mean rate of one every ~60 years. Large earthquakes are documented back to 1 A.D. [*Ambraseys*, 2002] (Figure 1), but damage descriptions from broadly distributed geographic locations begin with the 1509 Marmara Sea earthquake [*Ambraseys and Finkel*, 1990, 1991, 1995]. These observations are required for the quantitative approach to historic earthquake locations and magnitudes used here.

2.1. Methods

[7] Published accounts of damage caused by Marmara Sea earthquakes [*Ambraseys and Finkel*, 1990, 1991, 1995] were interpreted on the Modified Mercalli intensity (MMI) scale for eight earthquakes from A.D. 1500 to 2000 (Table 1) [*Parsons et al.*, 2000]; earthquakes in 1912 and 1999 were included for test purposes because instrumental locations

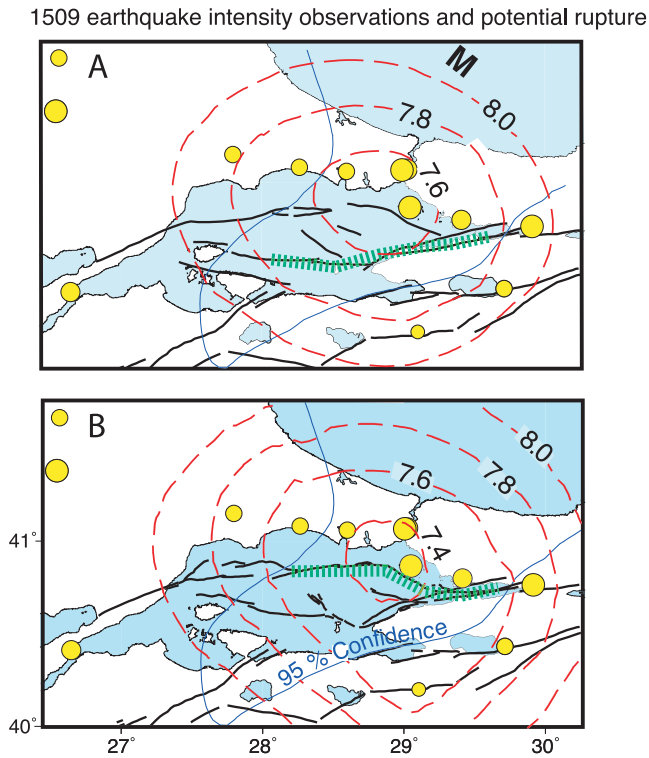

Figure 2. MMI observations used to locate and estimate the size of the 10 September 1509 earthquake with different fault maps and attenuation relations using (a) the map of *Parke et al.* [1999] and the attenuation relation of *Bakun and Wentworth* [1997] and (b) the map of *Armijo et al.* [2002] and the attenuation relation of *Ambraseys* [2002]. The result is that the 1509 earthquake was assigned to a completely different fault segment by *Parsons et al.* [2000] (Figure 2a) than in this study (Figure 2b).

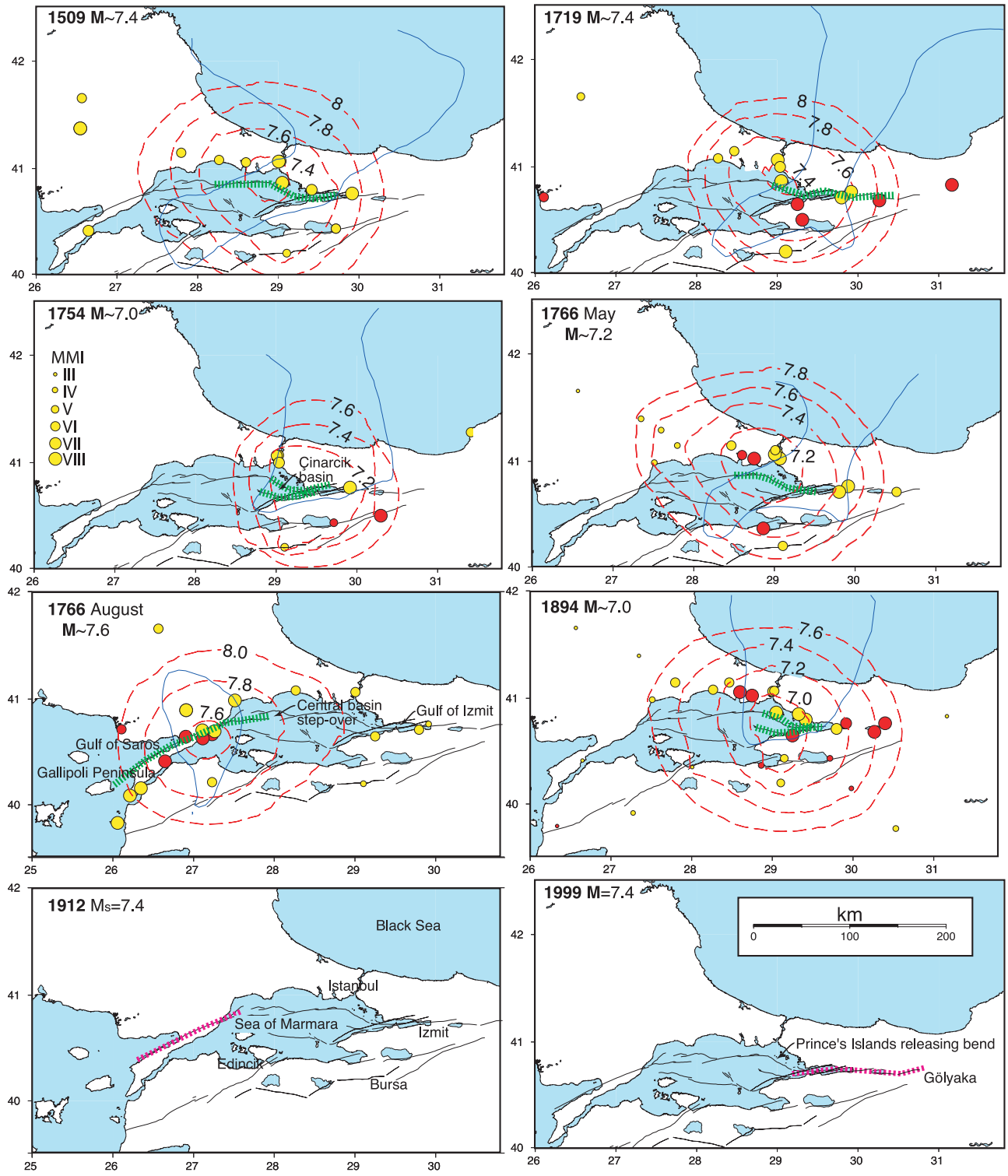

Figure 3. A.D. 1500–2000 earthquake catalog for the Sea of Marmara region. The events between 1509 and 1894 were located using MMI values estimated from damage descriptions compiled by *Ambraseys and Finkel* [1990, 1991, 1995] (Table 1). Estimated ruptures are shown by the thick dashed green lines. MMI values are shown by yellow dots (red dots are sites of damage potentially enhanced by soft sediments). A further description of these events is provided in Appendix A.

Table 1. Modified Mercalli Intensity (MMI) Assignments From Damage Descriptions Compiled by *Ambraseys and Finkel* [1990, 1991, 1995]

	Earthquake Date							
	1509	1719	1754	1766a	1766b (5 Aug.)	1894 (10 July)	1912 (9 Aug.)	1999
Reported deaths	>5000	6000	2000	5300	>5000	1300	>2000	
Major tsunami	Izmit Bay			Izmit Bay				
Observations	19	18	11	19	30	43	26	19
MMI by site name								
Adapazari						8		9
Akyazi								8.5
Ankara			3			3		3
Avlonya						3		
Aydin					3	3		
Aytos				3				
Balkans					3			
Bandirma						5.5		
Bilecik						5.5		
Bolu	7.5					4	3	7
Bosphorous	7.5		7.5	8		7		6
Bozcaada				3.5	8	3		
Bucharest						3	3	
Burdur						3		
Bursa	6.5	8	6.5	7	6	6.5	5	6
Büyükçakmece	7			7		8		
Cairo	3							
Çanakkale					8		8	
Çatalca		7		7		7		
Chalkis (Greece)						3		
Çorlu	7			6		7	7	
Danube basin	3				3			
Dimetoka	8.5							
Düzce		9.5				4		8
Edirne	7	6.5	4	5	7	5	6	
Edremit							6	
Enez		7			7		8	
Eregli			7					
Eskisehir						6		4
Evrese					8.5			
Ezine						4		
Galata/Pera				8				
Gazikoy					9	5	9	
Gebze	8.5					8		7.5
Gelibolu	7.5				9	5	9	
Gemlik						6.5		
Geyve			8.5					
Golyaka								9
Gülcük (on fault)					9			9.5
Hora					9.5			
Imroz							8	
Istanbul	9	8	7.5	8.5	7	7.25	6	6
Izmir		4	4	3	3		3	
Izmit	9	9.5	8	8.5	6	7.5	5	8.5
Iznik	7		6.5			6	5	6
Karamürsel		9.5		8	7	7.5		8
Karisdiran				6			7	
Kartel/Pendik						8		
Kilidbahir					8			
Konya						3		
Korfez								8
Küçükçekmece				8		8		8
Lüleburgaz				6		5	7	
Malkara					8			
Mitilini					7			
Mount Athos	3	3			3			
Mudanya				8		6		
Mudunru						4		
Mürefte					9		9	
Mustafakemalpasa						4		
Orhangazi		8.5						6
Prince's Islands	8	7.5				8		
Sapanca		9.5				9		8
Sarkoy					9		9	
Seddulbahir					8		8	

Table 1. (continued)

	Earthquake Date							
	1509	1719	1754	1766a	1766b (5 Aug.)	1894 (10 July)	1912 (9 Aug.)	1999
Siebenburg	3							
Silivri	7					7		
Silivri (north of)		7						
Sofia (Bulgaria)						3	3	
Sopron					3			
Tanem	3							
Tekirdag				6	8.5	6	8	
Thasos							6	
Thessaloniki		4		3	3		3	
Üsküdar		7.5	7.5					
Vienna					3			
Yalova		10			7	8.5	5	8
Yannina (Iannina)						3		
Yenice						5.5		
Yesilkoy/St. Stephano						7.5		

and magnitudes are available. MMI values were assigned to 200 damage descriptions (Table 1), and the method of *Bakun and Wentworth* [1997] was used to infer M and epicentral location from MMI through an empirical attenuation relation. The original relation used by *Bakun and Wentworth* [1997] is

$$M_i = (\mathrm{MMI}_i + 3.29 + 0.0206 d_i)/1.68, \quad (1)$$

where d_i is distance in km between intensity (MMI) observation and epicenter, and was developed from 30 California shocks with both intensity and instrumental observations. This expression was replaced in this study by

$$M_{si} = -1.54 + 0.65(\mathrm{MMI}_i) + 0.0029 d_i + 2.14 \log(d_i), \quad (2)$$

where moment magnitude (M) is determined from surface wave magnitude (M_s) using

$$\log(M_i) = 16.07 + 1.5 M_{si} \quad (3)$$

[*Ambraseys*, 2002]. The RMS fit to this relation is calculated for trial locations on a 5 × 5 km-spaced grid. Felt reports (MMI < IV) were excluded and MMI > VIII observations were saturated to VIII because criteria for higher intensities involve observations other than building damage, and because for poorly constructed, or degraded masonry, damage may be total at MMI = VIII. The *Bakun and Wentworth* [1997] method uses a grid search for an intensity center; thus distance in equation (1) is to a point source. However in the near field and for the largest MMI values, distance (d_i) in the attenuation relation of *Ambraseys* [2002] is not epicentral, but is instead the nearest distance to the earthquake rupture plane. Far from the fault rupture, distances between an intensity observation point and any point along the rupture are not substantially different. This is not true very close to the rupture plane, thus equation (2) cannot be used in the *Bakun and Wentworth* [1997] method, and equation (1) is used instead. *Ambraseys* [2002] provided criteria for where equation (2) is epicentral, which are adopted here, and investigated the differences between equation (1) and equation (2), which do not tend to be large in the near field.

[8] The input MMI values yield an output grid of moment magnitudes and confidence intervals. The historical earthquake rupture most consistent with the MMI data would be the one that minimizes M and falls within 95% confidence bounds on minimized misfit to input MMI values. The historical earthquake rupture must be associated with a fault; the segment nearest the zone of minimum magnitude of sufficient length to accommodate the rupture is identified as the earthquake source. Additionally, the rupture is centered in the 95% confidence interval (Figures 2 and 3).

[9] The historic earthquake location process is highly dependent on the input data. *Parsons et al.* [2000] located historic Marmara Sea events with a map by *Parke et al.* [1999] (based on seismic reflection profiles), estimated rupture lengths and the mean slip from empirical relations on M for continental strike-slip faults [*Wells and Coppersmith*, 1994], and used the original attenuation relation of *Bakun and Wentworth* [1997] (equation (1)). In this study the new map of *Armijo et al.* [2002] is used, which is based on multibeam bathymetry, and which shows more continuous strike-slip fault segments (Figure 2). Surface rupture lengths along the North Anatolian fault [*Barka*, 1996] are found to be longer than the global mean of *Wells and Coppersmith* [1994], exceeding one standard deviation (Figure 4). The combined use of the new fault map, the new regression of rupture length and M, and the new attenuation relation (equation (2)) leads to different historic earthquake location from MMI values. For example, *Parsons et al.* [2000] calculated the 1509 earthquake to have been $M \sim 7.6$, and located the event on a combination of interpreted strike-slip and normal faults in the southern Sea of Marmara (Figure 2a). In this study the event is $M \sim 7.4$, and is located on a more continuous segment of the North Anatolian fault in the north Sea of Marmara (Figure 2b). These differences have important ramifications for earthquake interevent times and time elapsed since the last rupture of a given fault segment.

[10] Marmara Sea earthquakes associated with both intensity and instrumental data were used to test the location technique (Figure 5). These include the 1912 M_s = 7.4 Saros-Marmara (360 intensities [*Ambraseys and Finkel*, 1987]), 1963 M_s = 6.4 Yalova (11 intensities [*Ambraseys*,

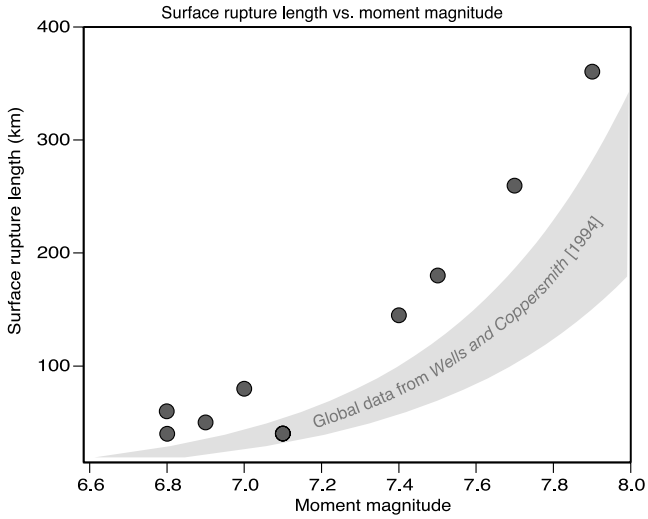

Figure 4. Comparison of surface rupture length (solid circles) to moment magnitude (M) observed along the North Anatolian fault [*Barka*, 1996] with the global data of *Wells and Coppersmith* [1994] (the $\pm 1\sigma$ range is plotted as the shaded zone). All but one North Anatolian rupture exceed the range of global observations.

1988]), and 1999 M = 7.4 Izmit earthquakes (185 intensities). For the 1912 and 1999 events, 50 sets of 25 intensities were randomly selected (the mean number for the historical shocks) to calculate epicentral and magnitude errors. This yields intensity centers within ±50 km (at 95% confidence) of the instrumental epicenters, and gives the correct M or M_s within ±0.3 magnitude units. Site corrections were not made because no tendency for epicenters to be pulled toward sedimentary sites was found, and because improvement was only found by *Bakun and Wentworth* [1997] when detailed site geology was available.

[11] Although necessary to make time-dependent probability calculations, assignment of historical earthquakes to particular fault segments represents a major assumption that is subject to unquantifiable errors in the forecast. Three efforts are made to account for possible assignment errors: (1) earthquake locations and seismic strain are tested against the geodetically measured interseismic strain rate, (2) regional Poisson probability calculations are made, which assume earthquakes occur randomly in time and space and are thus independent of the interevent model, and (3) varying degrees of randomness are introduced into the probability calculations by drawing from distributions of earthquake interevent times that allows for possible errors in the interevent model. These efforts are discussed in detail in sections 2.3 and 2.4.

2.2. Catalog Events and Interevent Model

[12] The A.D. 1500–2000 Marmara Sea catalog consists of 9 large earthquakes (Figure 3) that are used to build interevent and elapsed times for use in probability calculations. Six of these events (1509–1894) were relocated and assigned magnitudes from MMI values determined from damage descriptions [*Ambraseys and Finkel*, 1990, 1991, 1995]. The two most recent events (1912, 1999) have instrumental locations and magnitudes. A full discussion of these earthquakes, their assigned locations, and their calculated magnitudes can be found in Appendix A.

[13] Assignment of historical earthquakes to faults (Figure 3) indicates possible repeated rupture of some segments. The 10 September 1509 $M \sim 7.4$ and the 22 May 1766 $M \sim 7.2$ earthquakes appear to have broken the same fault segment (called Prince's Islands segment here (Figure 1)) except that the smaller 1766 event did not reach as far west as did the 1509 shock (Figure 3). The 25 May 1719 $M \sim 7.4$ and 17 August 1999 M = 7.4 Izmit earthquakes both appear to have ruptured the Izmit segment (Figure 1) of the North Anatolian fault (Figure 3). The 5 August 1766 $M \sim 7.6$ and the 13 September 1912 M_s = 7.4 earthquakes both broke the North Anatolian fault along the Gallipoli Peninsula (Ganos segment (Figure 1)) (Figure 3). From these patterns, interevent and elapsed times can be estimated for three major North Anatolian fault segments by using the observed time difference between events and the open intervals at the beginning and end of the 500 year interval between A.D. 1500 and 2000 (Table 2).

[14] To account for open intervals, interevent times for fault segments were calculated using a Monte Carlo technique. Earthquake times were repeatedly drawn at random from probability density distributions of varying means over a 2000 year period; distributions that could reproduce observed earthquake times for each fault segment within the last 500 year part of the sequence were tracked, and the mean of all distributions that fit the observations was used in the recurrence model. The probability density function used was the Brownian passage time model [*Matthews et al.*, 2002] given by

$$f(t,\mu,\alpha) = \sqrt{\frac{\mu}{2\pi\alpha^2 t^3}}\exp\left(-\frac{(t-\mu)^2}{2\mu\alpha^2 t}\right), \qquad (4)$$

where μ is the average interevent time and α is the aperiodicity, equivalent in concept to the coefficient of variation (COV; standard deviation divided by the distribution mean) in a normal distribution. Distributions with α = 0.5 were used to model interevent times. The Brownian distribution is also used in this study to make time-dependent probability calculations (see section 2.4).

[15] Incorporation of information represented by the open intervals usually causes calculated interevent times to be longer than the time difference between a pair of earthquakes observed within the 500 year window. For example, Brownian distributions with means ranging from 167 to 411 years could recreate the 257 year time difference (1509–1766) between earthquakes fixed in the A.D. 1500–2000 interval on the Prince's Islands fault using Monte Carlo simulations. Thus the mean interevent time for the Prince's Islands segment is calculated to be 270 years. Similarly, the 1766 and 1912 events on the Ganos fault could be fit by distributions centered between 182 and 236 years, leading to a 207 year mean interevent time (Table 2). The Izmit segment was calculated to have a mean 288 year interevent time and could be fit by a range of models from 188 to 442 years.

[16] Complicating the interevent model are the 10 May 1556 $M_s \sim 7.1$, 2 September 1754 $M \sim 7.0$, and 10 July 1894 $M \sim 7.0$ earthquakes. These smaller events were

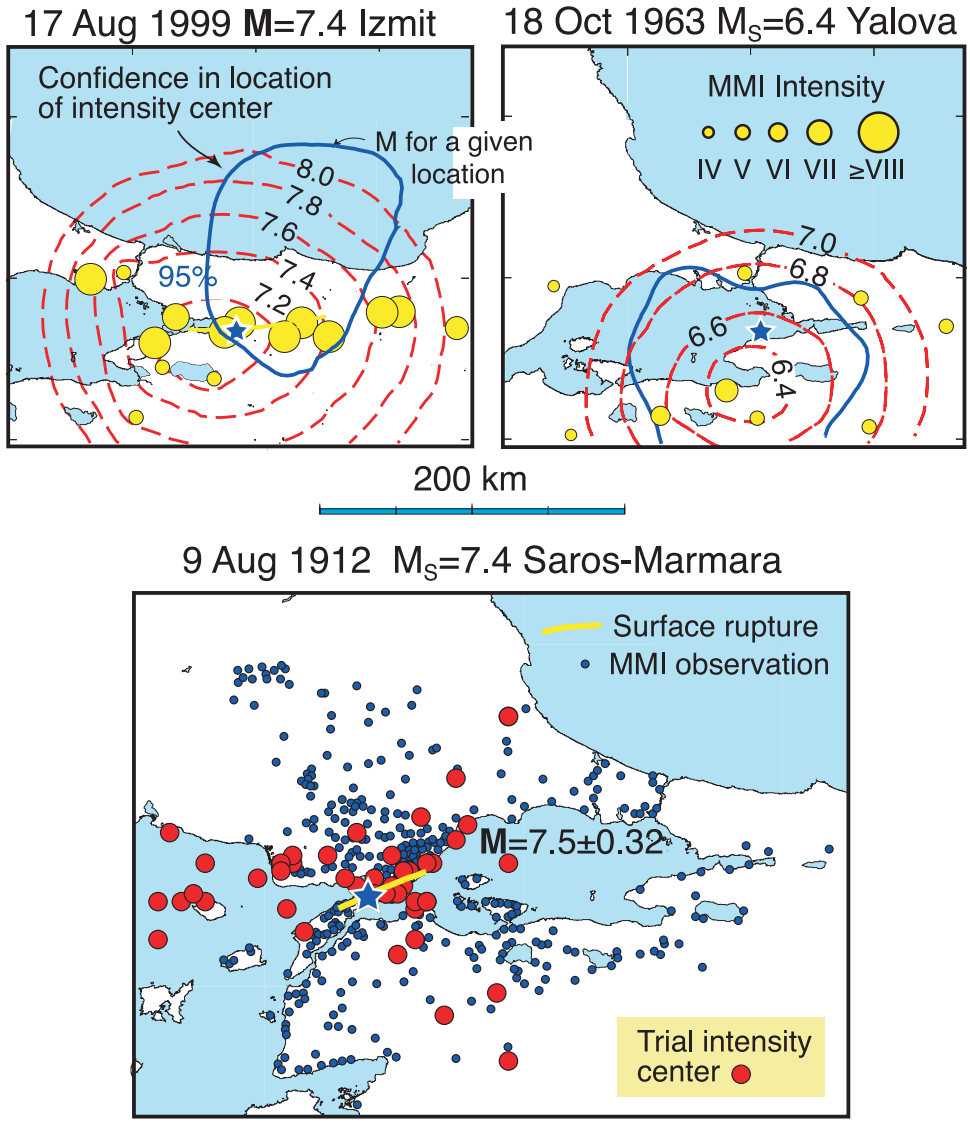

Figure 5. A test of the *Bakun and Wentworth* [1997] method modified with the *Ambraseys* [2002] attenuation relation using the 1999, 1963, and 1912 Marmara Sea earthquakes (each with known locations and magnitudes). For the 1912 event, 50 sets of 25 intensities (the mean number for the historical shocks) were selected at random to calculate epicentral and magnitude errors. This yields intensity centers within ±50 km (at 95% confidence) of the instrumental epicenters and gives the correct M or M_s within ±0.3 magnitude units.

assigned locations in the Çinarcik basin or southern Sea of Marmara on mapped normal faults (Figure 3) (Appendix A), although they could have occurred on the North Anatolian fault. These $M \sim 7.0$ earthquakes are treated as independent sources in the interevent model, with an observed mean frequency of 170 years (Table 2). A Monte Carlo simulation was conducted for these events in the same manner as for the other Sea of Marmara faults except that earthquake

Table 2. Interevent Model for Sea of Marmara Fault Segments From the Catalog Shown in Figure 3[a]

Fault	Events	Observed Δtime in A.D. 1500–2000 Interval	Model Interevent Time, Including Open Intervals, years	Elapsed Time, years	Magnitude (M)
Ganos	1766, 1912	146	~207	92	~7.5
Prince's Islands	1509, 1766	257	~270	238	~7.3
Izmit	1719, 1999	280	~288	5	~7.4
Çinarcik basin $M \sim 7$ events	1556, 1754, 1894	169	~250		~7.0

[a]Segment locations are shown in Figure 1. The use of "floating" $M \sim 7$ events refers to potential normal-fault earthquakes that may have occurred on different fault segments in or around the Çinarcik basin. These events may not repeat on the same faults and are treated as occurring randomly in time about a mean interevent time of 250 years (Poisson model).

times were drawn from an exponential, or Poisson distribution (random in time), which indicated that a ~250 year interevent time for these earthquakes best reproduces their occurrence over the A.D. 1500–2000 interval.

2.3. Catalog Evaluation and Discussion

2.3.1. Catalog Seismic Strain Versus Geodetic Strain

[17] One means of investigating the A.D. 1500–2000 Sea of Marmara earthquake catalog is to balance seismic strain with the geodetically measured interseismic strain rate. No direct observations are available on the amount of coseismic slip associated with the historic events in the A.D. 1500–2000 catalog, so the global regressions of *Wells and Coppersmith* [1994] must be used; observations elsewhere along the North Anatolian fault zone indicate that the amount of slip and surface rupture lengths tend toward the high range of the global compilations [*Barka*, 1996] (Figure 4), perhaps because of a shallow locking depth [e.g., *Meade et al.*, 2002]. Thus regressions of mean slip at the $+1\sigma$ range are compiled and compared.

[18] Few GPS observations can be made in the Sea of Marmara, so there is uncertainty about the relative strain accommodated by the northern strand of the North Anatolian fault beneath the Sea as compared with the fault strand south of the Sea. A block model fit to the available GPS data indicates that the northern strand may accommodate 23 ± 2 mm/yr compared with ~5 mm/yr on the southern strand [*Meade et al.*, 2002; *Le Pichon et al.*, 2003]. Coseismic strain estimated from the A.D. 1500–2000 earthquake catalog is ~20 mm/yr on the Ganos segment (1 $M \sim 7.4$ and 1 $M \sim 7.6$ yielding 9.8 m slip over 490 years), ~13 mm/yr on the Prince's Islands segment (1 $M \sim 7.2$, and 1 $M \sim 7.4$ yielding 6.5 m slip over 490 years), and ~23 mm/yr on the Izmit segment (2 $M \sim 7.0$, and 2 $M \sim 7.4$ yielding 11.2 m slip over 490 years). In that model there is a significant slip deficit on the Prince's Islands segment. If slip from the $M \sim 7.0$ shocks (2 September 1754 and 10 July 1894) are assigned to the Prince's Islands segment, then the slip rates change to ~20 mm/yr on the Prince's Islands segment and ~16 mm/yr on the Izmit segment. The last possibility has the 2 $M \sim 7.0$ events split between the Prince's Islands and Izmit segments yielding ~16 mm/yr on the Prince's Islands segment and ~19 mm/yr on the Izmit segment. In all cases there appears to be a slip deficit somewhere beneath the Sea of Marmara (unless aseismic creep accommodates it), most likely on the Prince's Islands segment, which has not produced a $M > 7.0$ earthquake since 1766 (Table 2); a similar conclusion was reached by *Hubert-Ferrari et al.* [2000].

2.3.2. Regional Poisson Probability Comparison and Catalog *b* Value

[19] A Poisson probability model is one that treats earthquakes as random in time (t) about a mean recurrence interval (μ) as

$$P(t \le T \le t + \Delta t) = 1 - e^{-\Delta t/\mu}. \quad (5)$$

This model can be applied to the A.D. 1500–2000 interevent catalog such that probabilities are calculated for each of the 4 interevent frequencies (Table 2), combined as

$$P = 1 - (1 - P_g)(1 - P_{pi})(1 - P_i)(1 - P_7), \quad (6)$$

(where P_g, P_{pi}, P_i, and P_7 are probabilities for the for Ganos, Prince's Islands, Izmit, and "floating" $M \sim 7.0$ segments), and compared with Poisson probability calculated from the A.D. 1–1500 catalog. The A.D. 1–1500 catalog does not have good locations, but does provide a lengthy record of strong shaking in the Marmara region, providing a standard for evaluation of the A.D. 1500–2000 catalog interevent model.

[20] If the 4 fault segments capable of generating $M \ge 7$ earthquakes (Table 2) are included in the A.D. 1500–2000 Poisson model, the combined 30 year probability is 38%. The A.D. 1–1500 catalog has 19 events located within, or adjacent to the Sea of Marmara assigned $M_s \ge 6.8$ by *Ambraseys* [2002], yielding a 79 year interevent time and a 30 year Poisson probability of 32%; the A.D. 1–2000 catalog has 28 events yielding a 71 year interevent time and a 30 year Poisson probability of 35%. Thus the interevent model determined from the A.D. 1500–2000 catalog is able to reproduce the most robust observational data, the 2000 year historical record of earthquake damage, to within 3–6%.

[21] An additional means of evaluating the A.D. 1500–2000 earthquake catalog is to calculate its b value. It is recognized that the magnitude distribution of the 500 year catalog is narrow, however if its b value varies significantly from independent observations, then this might be an indication of problems with the magnitude determinations. The A.D. 1500–2000 catalog b value is 1.4 by maximum likelihood [*Aki*, 1965]. The mean b value for the Sea of Marmara region from 1983 to 1999 is 1.3 according to *Öncel and Wyss* [2000].

[22] In summary, the A.D. 1500–2000 catalog has three sets of two $M > 7$ earthquakes that appear to have ruptured the same fault segments. Time separations between events and open intervals enable rough interevent times to be calculated for those ruptures. No event in the past 500 years appears to have broken the entire submerged North Anatolian fault [cf. *Le Pichon et al.*, 2001]; this does not mean that a $M \sim 7.6–8.0$ event is impossible, however *Ambraseys* [2002] found no evidence for such large events beneath the Sea of Marmara over the past 2000 years. Three $M \sim 7.0$ earthquakes also occurred beneath or adjacent to the Sea of Marmara that are more difficult to identify as recurrent, but appear necessary to account for plate boundary strain. However, there is significant uncertainty as to which part of the fault was strained by these events. Almost 240 years have passed since the last large earthquake on the Prince's Islands segment of the North Anatolian fault beneath the central Sea of Marmara; thus a moment deficit may have developed.

2.4. Regional Time-Dependent Probability

[23] In recognition that earthquakes are likely not completely random in time and space as the Poisson model assumes, time-dependent probabilities are calculated for the Sea of Marmara region. However, it is also recognized that earthquake occurrence is highly irregular, thus the effects of varying earthquake interevent times and aperiodicity are fully explored.

[24] A time-dependent probability calculation is based on the renewal hypothesis of earthquake regeneration

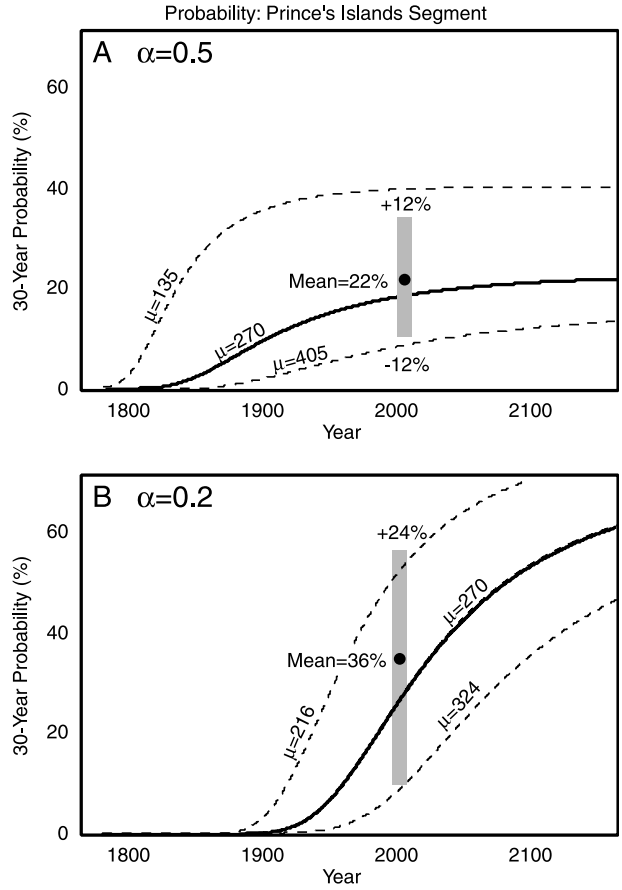

Figure 6. Comparison of 30 year probability versus time for an earthquake on the Prince's Islands segment using aperiodicity (α) of (a) 0.5 and (b) of 0.2. The thick black lines are calculations made with the mean interevent time of 270 years from Table 2. The dashed lines are 50% perturbations from the mean (Figure 6a) or 20% perturbations (Figure 6b), meant to illustrate the approximate range pulled at random from Brownian distributed interevent times to estimate standard deviations (Table 3). The plots demonstrate how $\pm 1\sigma$ variations for $\alpha = 0.2$ can exceed those for $\alpha = 0.5$ in some circumstances.

wherein the likelihood of an earthquake on a given fault is lowest just after the last shock. As tectonic stress builds over time, the odds of another earthquake grow. A time-dependent probability calculation sums a probability density function $f(t)$ that mimics this tendency as

$$P(t \le T \le t + \Delta t) = \int_t^{t+\Delta t} f(t)dt, \tag{7}$$

where $f(t)$ can be any distribution, such as lognormal [e.g., *Nishenko and Buland*, 1987], Weibull [*Hagiwara*, 1974], or Brownian Passage Time [*Matthews et al.*, 2002]; the Brownian model is used in this study and is given by equation (4). The breadth of the chosen distribution is representative of the irregularity, or aperiodicity of earthquake recurrence.

[25] The A.D. 1500–2000 catalog is not adequate to estimate the aperiodicity (α) of interevent times directly, so I consider a range from a conservative value of 0.5 [*Working Group on California Earthquake Probabilities (WGCEP)*, 1999, 2003] to a more traditional value of 0.2 [e.g., *Nishenko and Buland*, 1987; *Ogata*, 1999; *Lindh*, 2004]. The Poisson probability calculations of section 2.3.2 represent an end-member of very high aperiodicity. The effects of aperiodicity on earthquake probability and its changes with time can be seen clearly in Figure 6, which shows that late in the earthquake cycle, small aperiodicity ($\alpha = 0.2$) leads to higher probability, whereas a broader distribution of interevent times ($\alpha = 0.5$) can yield higher values earlier in the cycle.

[26] Some insight into aperiodicity in the Marmara Sea region might come from examining variability in the moment of earthquakes thought to have ruptured the same segments. For example, the 10 September 1509 $M \sim 7.4$ and 22 May 1766 $M \sim 7.2$ earthquakes are treated here as recurrent events; if the calculated magnitudes are correct, the ratio of moment release for these two earthquakes is 0.501. The same result is obtained by comparing the 5 August 1766 $M \sim 7.6$ and 13 September 1912 $M_s = 7.4$ earthquakes. Thus if moment accumulation rate and variation in its release is a proxy for variation in earthquake periodicity, then perhaps $\alpha = 0.5$ is appropriate for Sea of Marmara probability calculations. A definitive conclusion cannot be reached because the potential errors in the magnitude calculations from historic earthquakes could be larger than the 0.2 magnitude unit variations between the compared events.

[27] Thirty year time-dependent earthquake probabilities were calculated for the three identified fault segments beneath the Sea of Marmara using the interevent times of Table 2 and aperiodicity values of $\alpha = 0.2$ and $\alpha = 0.5$ (Table 3). Additionally, a 30 year Poisson calculation was

Table 3. Earthquake Probability Calculations for Sea of Marmara Fault Segments Using the Interevent and Elapsed Times From Table 2[a]

		Time-Dependent		Interaction		Afterslip	
Segment	Poisson	$\alpha = 0.5$ (1σ)	$\alpha = 0.2$ (1σ)	$\alpha = 0.5$ (1σ)	$\alpha = 0.2$ (1σ)	$\alpha = 0.5$ (1σ)	$\alpha = 0.2$ (1σ)
Ganos	14	20 (±17)	6 (±12)	20 (±17)	7 (±13)	20 (±17)	7 (±13)
Prince's Islands	11	22 (±12)	36 (±24)	31 (±15)	54 (±26)	34 (±14)	62 (±25)
Izmit	10	~0	~0	~0	~0	~0	~0
Çinarcik $M \sim 7$	11	11	11	11	11	11	11
Combined	38	44 (±18)	46 (±23)	51 (±18)	62 (±28)	53 (±18)	69 (±28)
Istanbul	21	29 (±12)	43 (±24)	39 (±15)	59 (±26)	41 (±14)	66 (±25)

[a]Thirty year probability (%) in 2004. The probability of each segment of producing a $M \ge 7$ earthquake between 2004 and 2034 is calculated using Poisson, time-dependent, time-dependent with coseismic stress transfer from the $M = 7.4$ 1999 Izmit earthquake, and time-dependent with coseismic and postseismic stress transfer from the Izmit event. Reported probability values are the means of 1000 calculations using distributions of input parameters; the 1σ parameter sensitivities are found from the distribution of results.

made for "floating" $M \sim 7$ earthquakes based on three events identified between A.D. 1500–2000 (interevent time ~250 years), which is 11%. Reported time-dependent probability values are the means of 1000 calculations made per segment, with interevent times drawn at random from Brownian distributions about the modeled interevent times [*Savage*, 1991, 1992]. This process enables examination of parameter choices and calculation of standard deviations on probability values (Table 3). The ranges given on calculated probabilities are not formal uncertainties; rather they provide an understanding of the sensitivity to parameter choices.

[28] The Ganos segment of the North Anatolian fault last ruptured on 13 September 1912, and has a modeled interevent time of ~207 years. Trenches on the Ganos segment were used to calculate a mean interevent time of 350 years, longer than the modeled value, although periods of shorter interevent times of 150 years over the past several surface ruptures were noted [*Rockwell*, 2000], which match the event separation from the A.D. 1500–2000 catalog. The 30 year Poisson probability for this segment is 14%; the time-dependent calculation for this segment over the period 2004–2034 is 20 ± 17% if $\alpha = 0.5$ (reported sensitivities are one standard deviation, or 67% confidence), and 6 ± 12% if $\alpha = 0.2$. The Ganos segment (Figure 1) calculations are associated with the largest uncertainty relative to the probability values in this study because the short elapsed time since 1912 compared with modeled interevent time of 207 years causes the calculations to be particularly susceptible to small variations in interevent time.

[29] The Prince's Islands segment in the central Sea of Marmara (Figure 1) last ruptured on 22 May 1766, and is calculated to have a 270 year interevent time. Consequently, while the 30 year Poisson probability for this segment is 11%, the time-dependent calculation for 2004–2034 is higher at 22 ± 12% if $\alpha = 0.5$, and 36 ± 24% if $\alpha = 0.2$ (Table 3). The Izmit segment last ruptured on 17 August 1999; the interevent time was calculated to be 288 years, yielding a 30 year Poisson probability for this segment of 10%. The time-dependent calculation for 2004–2034 on the Izmit segment is ~0% because so little time has elapsed since the last rupture in 1999. The 30 year time-dependent segment probabilities can be combined using equation (5); if $\alpha = 0.5$, the probability of a $M \geq 7$ earthquake in the Sea of Marmara region (includes Ganos, Prince's Islands, Izmit, and "floating" earthquake sources) is 44 ± 18%. If $\alpha = 0.2$, the combined probability is nearly the same at 46 ± 23% (Table 3), although with greater parameter sensitivity.

[30] The distribution of possible interevent times is more limited if $\alpha = 0.2$, thus one might expect a smaller range of values in parameter sensitivity calculations. However, when α is smaller in time-dependent calculations, it causes the maximum probability to be larger. This in turn can lead to a wider range of possible probabilities. Additionally, at a given time, the spectrum of probabilities resulting from a distribution of interevent times depends on the slope of probability gain with time, which differs depending on α (Figure 6). Thus for Sea of Marmara time-dependent calculations, sensitivities on 30 year probability when $\alpha = 0.2$ can exceed those when $\alpha = 0.5$ (Figure 6).

[31] Of the identified fault segments beneath the Sea of Marmara capable of generating $M \geq 7$ earthquakes, the mean time-dependent probability is calculated to be significantly higher than the Poisson value only on the Prince's Islands fault. The combined time-dependent probability for all segments is nearly the same as the combined Poisson value (44% versus 38%) because the increased time-dependent probability on the Prince's Islands fault is offset by a decrease on the Izmit segment relative to the Poisson values (Table 3). One important distinction between the Poisson and time-dependent calculations is that under the time-dependent model, most of the hazard is associated with the Prince's Islands fault, which is the closest fault to highly populated Istanbul (Figure 1). The time-dependent 30 year probability for Istanbul is 29–43% compared with the Poisson calculation of 21% (Table 3). In the next two sections, the influence of the 17 August 1999 $M = 7.4$ Izmit earthquake on the probability of earthquakes beneath the Sea of Marmara will be calculated.

3. Stress Changes Caused by the 17 August 1999 $M = 7.4$ Izmit Earthquake

[32] The 17 August 1999 $M = 7.4$ Izmit earthquake killed 18,000 people, destroyed 15,400 buildings, and caused $10–25 billion in damage. However, the Izmit event is only the most recent in a largely westward progression of seven $M \geq 6.7$ earthquakes along the North Anatolian fault since 1939. Stress triggering has been invoked to explain the 60 year sequence of earthquakes rupturing toward Istanbul [e.g., *Ketin*, 1969; *Barka*, 1996; *Toksoz et al.*, 1979], in which all but one event promoted the next [*Stein et al.*, 1997]. An earthquake can be modeled as a slipping dislocation in an elastic half space [e.g., *Okada*, 1992], enabling estimation of stress transfer to other faults. Calculated changes in stress tensor components are resolved on planes of interest, and changes in failure stress are related to triggering or inhibition of future earthquakes. Usually the Coulomb stress change is calculated and used to explain patterns of seismicity [e.g., *Harris*, 1998, and references therein]. The Coulomb failure criterion ($\Delta\tau$) is defined by

$$\Delta\tau \equiv \left|\Delta\bar{\tau}_f\right| + \mu(\Delta\sigma_n + \Delta p), \tag{8}$$

where $\Delta\bar{\tau}_f$ is the change in shear stress on the receiver fault (set positive in the direction of fault slip), μ is the coefficient of friction, $\Delta\sigma_n$ is the change in normal stress acting on the receiver fault (set positive for unclamping), and Δp is pore pressure change.

[33] Globally, seismicity rates are observed to rise in regions of calculated stress increase and fall where the off-fault stress decreases [e.g., *Kagan and Jackson*, 1991; *Kagan*, 1994; *Parsons*, 2002a]. The $M = 7.4$ Izmit earthquake, as well as most background seismicity [*Ito et al.*, 1999], occurred where the failure stress is calculated to have increased 0.1–0.2 MPa by $M \geq 6.7$ earthquakes since 1939 [*Stein et al.*, 1997; *Nalbant et al.*, 1998; *Parsons et al.*, 2000]. The Izmit event, in turn, increased the stress beyond the east end of the rupture by ~0.1–0.2 MPa, where the $M = 7.2$ Düzce earthquake struck, and by 0.05–0.5 MPa beyond the west end of the 17 August rupture, where a

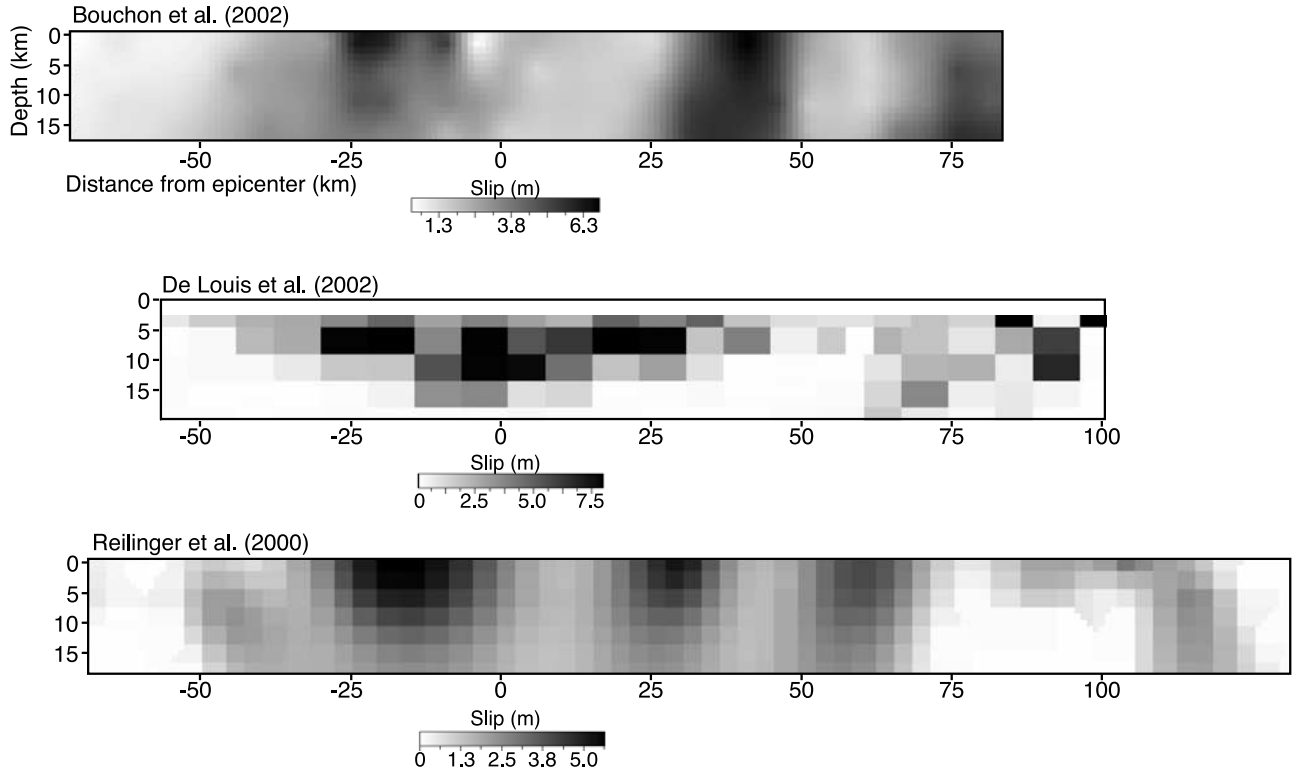

Figure 7. A comparison of modeled slip distributions of the 17 August 1999 $M = 7.4$ Izmit earthquake using combinations of teleseismic, strong ground motion, and geodetic data [*Reilinger et al.*, 2000; *Bouchon et al.*, 2002; *De Louis et al.*, 2002]. Dislocation models from these slip distributions were used to calculate coseismic static stress changes on Sea of Marmara faults.

cluster of aftershocks occurred [*Parsons et al.*, 2000]. The correspondence seen between calculated stress changes and the occurrence of large and small earthquakes, also reported by *Hubert-Ferrari et al.* [2000], strengthens the rationale for incorporating stress transfer into a seismic hazard assessment.

3.1. Slip Models

[34] Stress change calculations require a dislocation model of the perturbing earthquake, the 17 August 1999 $M = 7.4$ Izmit earthquake in this case. Preliminary stress change calculations were made not long after the Izmit shock that indicated stress increases on most Marmara Sea faults [*Hubert-Ferrari et al.*, 2000; *Parsons et al.*, 2000], using rough slip distribution estimates. As more time has passed since 1999, researchers have examined teleseismic, strong ground motion, and geodetic data [e.g., *Reilinger et al.*, 2000; *Bouchon et al.*, 2002; *De Louis et al.*, 2002; *Li et al.*, 2002], yielding more detailed slip models (Figure 7). In addition, studies of postseismic deformation [e.g., *Bürgmann et al.*, 2002; *Hearn et al.*, 2002] calculated deep afterslip beneath the coseismic rupture zone that may also affect Marmara Sea faults.

[35] Comparison of slip models determined from diverse data sources shows differences in the extent of the rupture and slip distribution (Figure 7). These variations cause different stress change values to be resolved on the Marmara Sea fault model (Figure 8). The exercise is useful because variability caused by uncertainty in Izmit earthquake coseismic slip can be examined and accounted for in probability calculations.

3.2. Coseismic Stress Changes

[36] To resolve stress on individual fault planes I used the program, DLC, written by R. Simpson (based on the subroutines of *Okada* [1992]) to calculate changes in the stress tensor at points along specified receiver fault surfaces caused by slip in the different Izmit earthquake source models in an elastic half space. For resolved stresses, no tectonic stress is applied; instead the strike, dip, and rake of the receiver faults are assumed. Post-Izmit microseismicity rate changes were best matched using low to intermediate friction coefficients ($\mu = 0.2-0.4$) on the Marmara Sea receiver faults [*Parsons et al.*, 2000], and a value of $\mu = 0.4$ was adopted for this study for use in equation (8).

[37] Calculated Coulomb stress changes at seismogenic depths (4–12 km) on Marmara Sea faults are mostly increased by the Izmit event (Figure 8). Maximum stress changes ($\Delta\tau \sim 0.5$ MPa) occur near the termination of rupture at the Hersek Peninsula, on the Prince's Islands segment and on faults in the Çinarcik basin. The influence of the Izmit earthquake diminishes to the west, only slightly increasing stress on the Ganos segment (Figure 8). Stress was reduced on faults parallel to the Izmit rupture on the southern branch of the North Anatolian fault, causing a likely delay in earthquakes there (Figure 8). The coefficient of variation (COV) on coseismic stress change beneath the

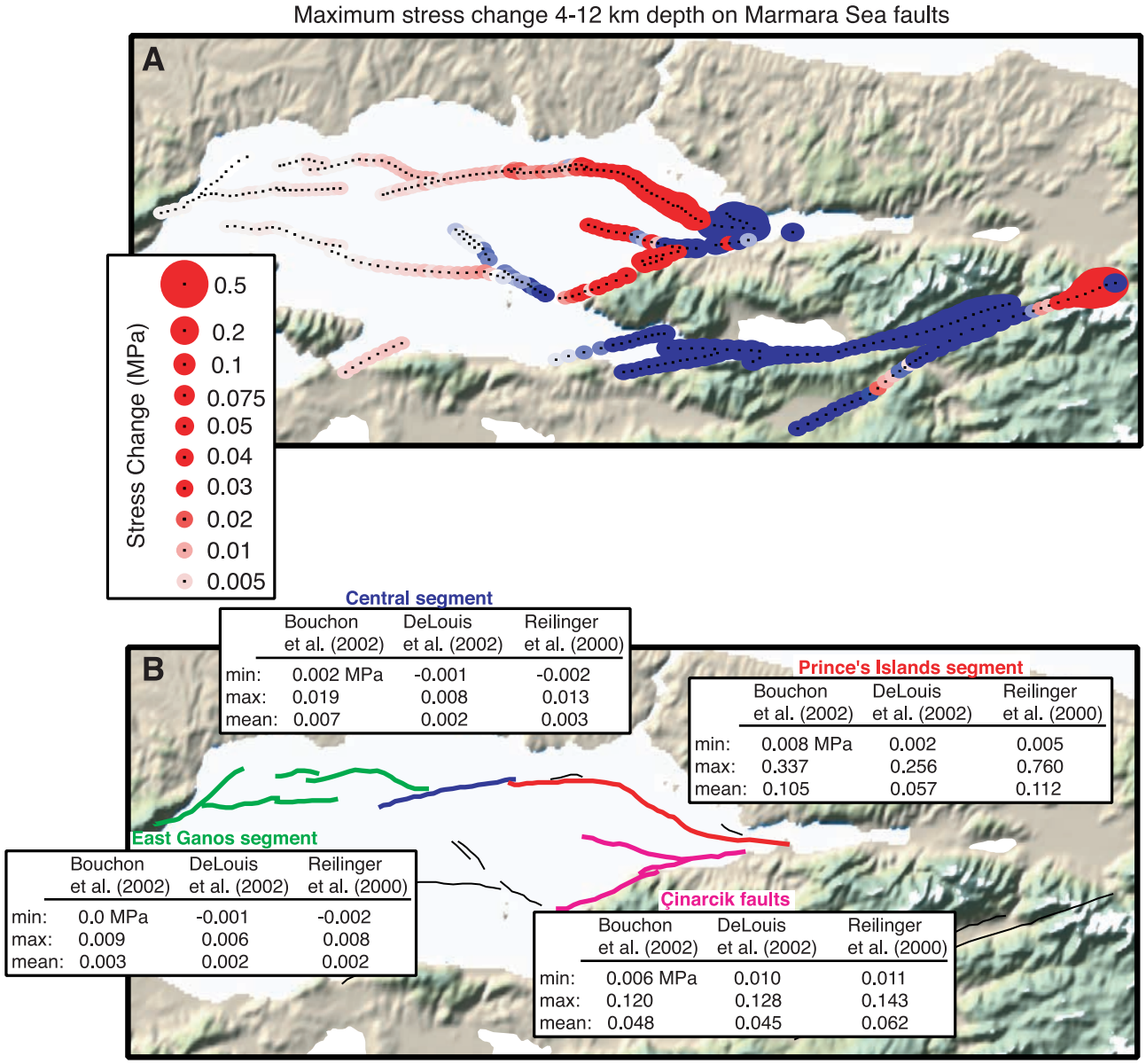

Figure 8. (a) Calculated coseismic Coulomb stress changes resolved on Sea of Marmara faults in the seismogenic crust. Stress increases are indicated by red dots, and decreases are indicated in blue. (b) Results using different slip distributions of the 17 August 1999 $M = 7.4$ Izmit earthquake are tabulated by segment.

Sea of Marmara is 0.35, and the mean stress change on Marmara Sea faults is a 0.04 MPa stress increase.

3.3. Postseismic Stress Changes

[38] Measured surface deformation following the 17 August 1999 Izmit earthquake was best fit with models that included postseismic afterslip in addition to viscous creep in the lower crust and/or upper mantle [e.g., *Hearn et al.*, 2002; *Bürgmann et al.*, 2002]. Significant afterslip can be modeled as dislocation slip that may have caused additional stress changes on Marmara Sea faults. To incorporate the effects of afterslip in probability calculations, the coseismic slip model of *Reilinger et al.* [2000] was first used to model the coseismic stress changes on Marmara Sea faults, and was then followed by the postseismic slip model of *Bürgmann et al.* [2002], because the afterslip model was generated from the coseismic slip of the *Reilinger et al.* [2000] distribution. The impact of afterslip is mostly limited to the Prince's Islands segment of the North Anatolian fault and to faults in the Çinarcik basin (Figure 9), where the mean stress change is about 0.05 MPa.

4. Incorporating 1999 $M = 7.4$ Izmit Earthquake Stress Changes Into Earthquake Probability Calculations

4.1. Methods

4.1.1. Static Probability Change

[39] An earthquake that occurs near another fault may advance or delay an impending earthquake by a time

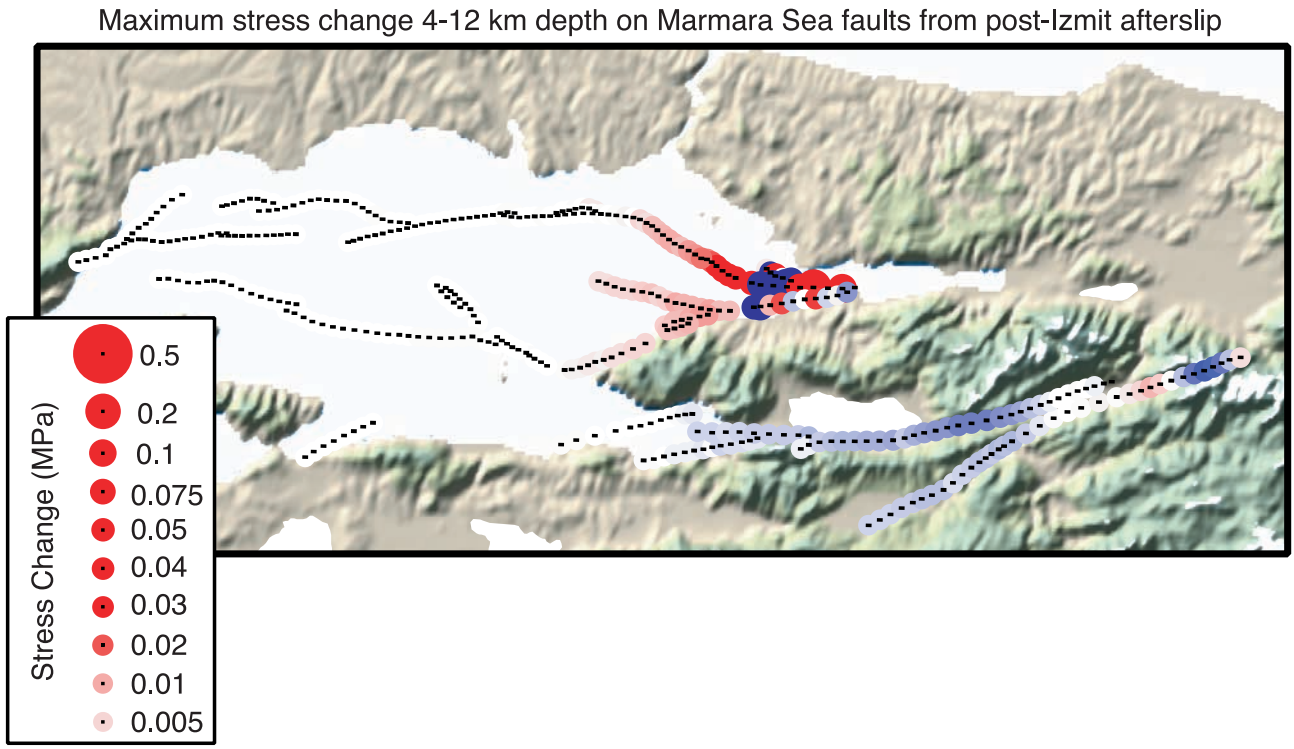

Figure 9. Calculated postseismic Coulomb stress changes resolved on Sea of Marmara faults in the seismogenic crust using the postseismic slip model of *Bürgmann et al.* [2002]. Postseismic slip is calculated to affect only the eastern Sea of Marmara faults.

proportional to the change in stress. The advance or delay, termed a clock change, or static probability change (T'), can be estimated by dividing the stress change ($\Delta\tau$) by the tectonic stressing rate ($\dot{\tau}$), as $T' = \Delta\tau/\dot{\tau}$. A simple way to incorporate earthquake interaction into time-dependent probability calculations is to accrue probability from the last earthquake time adjusted by the clock change ($T_0 + T'$) [e.g., *WGCEP*, 1990]. Alternatively, the earthquake recurrence interval γ can be adjusted by the clock change as $\gamma = \gamma_0 - T'$.

4.1.2. Transient Probability Change

[40] Recognized for more than 100 years, a temporary seismicity rate increase that decays inversely with time [*Omori*, 1894] results from stress changes [*Dutton*, 1904] caused by an earthquake. The Omori law decay in the rate of aftershocks is one of the few reliably time-predictable patterns of earthquake occurrence, and may be space predictable as well [e.g., *Stein*, 1999; *Parsons*, 2002a]. That increased seismicity rates are linked to the occurrence of a main shock is not a subject of reasonable debate. However, the physics of the process [e.g., *Scholz*, 1968; *Dieterich*, 1994; *Marcellini*, 1997; *Kilb et al.*, 2002; *Felzer et al.*, 2003] and the best means of incorporating the phenomenon into earthquake probability calculations [e.g., *Dieterich and Kilgore*, 1996; *Matthews et al.*, 2002; J. Gomberg et al., unpublished data, 2004] remain open questions.

[41] A persistent challenge in interaction probability is how best to incorporate the robust observations of Omori's law into a numerical representation of earthquake probability. Such observations are pertinent to the North Anatolian fault, where Omori law decay appears to govern the occurrence of large triggered earthquakes. If the thirteen $M \geq 6.8$ North Anatolian earthquakes for which the stress at the future epicenter was increased by $\geq$0.05 MPa [*Stein et al.*, 1997] are stacked in time bins as a function of the delay between the triggering and subsequent earthquakes [*Parsons et al.*, 2000] (Figure 10), they show an annual rate that decays as t^{-1} in a manner identical to aftershocks. Here I adopt the methodology of *Dieterich and Kilgore* [1996], which applies a rate- and state-dependent model to capture this phenomenon [*Dieterich*, 1994]. The methods for incorporating rate-state transients into probability calculations are given in Appendix B; important ramifications and assumptions inherent to the method are discussed below.

[42] The rate-state transient effect incorporates the enhanced rate of earthquake nucleation resulting from a stress increase, and can be expressed as a probability. For a stress decrease, the rate of nucleation declines, and eventually recovers (Appendix B). There are advantages in using the rate-state model, though a number of important assumptions must also be made. Rate-state friction laws describe physical processes that govern rock friction behavior in the laboratory setting. Most of the assumptions evolve from extrapolation to natural faults, and from presupposing stress conditions and distributions on natural faults. Under the *Dieterich* [1994] model, a group of faults or even a single fault is considered an infinite population of earthquake nucleation sites that are near to failure. These conditions are treated as Poissonian [*Dieterich and Kilgore*, 1996], are independent of the fault rupture history, and are applied on top of the static probability change (clock change of

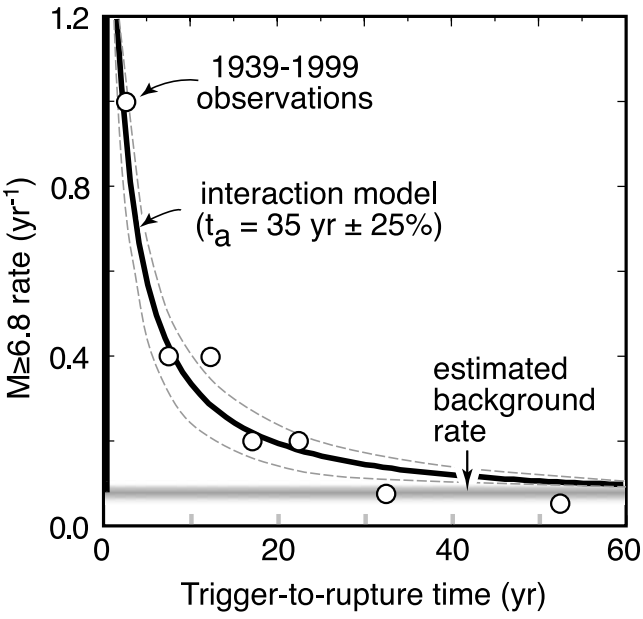

Figure 10. Transient response of the large earthquake rate to stress transfer on the North Anatolian fault [*Parsons et al.*, 2000]. Thirteen $M \geq 6.8$ North Anatolian earthquakes, for which the stress at the future epicenter was increased by $\geq$0.05 Mpa [*Stein et al.*, 1997], are plotted as a function of time. The earthquake rate decays as t^{-1} in a manner identical to aftershocks, as predicted by *Dieterich* [1994] and as observed globally by *Parsons* [2002a]. The time required to return to background rate is ~35 years on the North Anatolian fault.

section 4.1.1). Thus application of the model for earthquake probability of a given size to faults that have recently ruptured implies that, despite an expected stress drop caused by the recent earthquake, there still are an infinite number of potential rupture sites on the fault plane capable of generating the same-sized earthquake.

[43] Applying the rate-state model to probability calculations in the Marmara Sea region means that if there is not an infinite population of $M \geq 7$ nucleation sites along the North Anatolian fault, or if a $M \geq 7$ earthquake has occurred recently relative to the interevent time on a given fault, then the peak transient probability values could be overstated (J. Gomberg et al., unpublished data, 2004). Additionally, regionally applied rate-state parameters (see section 4.1.3) imply significant heterogeneity of fault zone conditions along the North Anatolian fault. At present, knowledge of fault zones nucleation populations is insufficient to gauge how many $M \geq 7$ sites exist, which is reflected by choosing broad distributions of parameters for use in the probability calculations made here. I adopt the *Dieterich and Kilgore* [1996] formulation because it captures observations of Omori decay following stress perturbations like the Izmit earthquake, and is derived from observations of laboratory rock physics. In addition, two previous reports of regional earthquake probability [*Stein et al.*, 1997; *Parsons et al.*, 2000] have applied the same methods, which enables results from this study to be directly compared.

4.1.3. Summary of Needed Parameters

[44] In addition to the interevent time, aperiodicity, and elapsed time on each fault, an interaction probability calculation that incorporates static and transient effects requires values for the stress change caused by the 17 August M = 7.4 Izmit earthquake ($\Delta\tau$), an observed aftershock duration (t_a), the combination of normal stress and constitutive constant $A\sigma$ (see Appendix B), and the secular stressing rate ($\dot{\tau}$) on a receiver fault. The A.D. 1500–2000 earthquake catalog permits rough estimates of the first three parameters as discussed in section 2.6. The mean coseismic and postseismic stress changes can be calculated as discussed in sections 3.2 and 3.3. The aftershock duration (t_a), $A\sigma$, and secular stressing rate ($\dot{\tau}$) are related by

$$\dot{\tau} = \frac{A\sigma}{t_a} \tag{9}$$

for nucleation sites that are close to failure [*Dieterich*, 1994]. Thus only two of the three remaining parameters must be determined. A regional aftershock decay time for large ($M \geq 6.7$) earthquakes was found by *Parsons et al.* [2000] from the 1939–1999 triggered earthquake sequence along the North Anatolian fault to be ~35 years (Figure 10). Empirical determination of the combined parameters $A\sigma$ requires comprehensive network coverage so that microseismicity rates can be measured [*Toda et al.*, 1998]. The Sea of Marmara makes such coverage impossible along the submerged North Anatolian fault; thus in this study the secular stressing rate on the Marmara Sea faults is calculated using a finite element model, and Aσ is found using equation (9).

4.2. Secular Stressing Rate From Finite Element Modeling

[45] The fault-stressing rate is required to estimate the clock change for static probability change as discussed in section 4.1.1, and it is needed for the transient probability change as discussed in section 4.1.3. A model that replicates observed strain measurements and has realistic rheology is required to estimate the stressing rate [*Parsons*, 2002b].

4.2.1. Finite Element Model

[46] The finite element model of the Sea of Marmara region (Figure 11) has three compositional layers inferred from measured crustal velocity structure [e.g., *Horasan et al.*, 2002; *Nakamura et al.*, 2002]. The upper 12.5 km of the model are crustal rocks approximated by wet Westerly granite [*Hansen and Carter*, 1983]. The 12.5-km-thick lower crust has elastic properties representative of basalt-diabase composition [*Caristan*, 1982]. The 45-km-thick upper mantle layer is required to maintain isostatic balance with the crustal column at sea level [*Lachenbruch and Morgan*, 1990], and has properties associated with a combination of wet and dry dunite samples [*Jackson*, 2002; *Carter and Tsenn*, 1987]. The model edges are oriented parallel and orthogonal to the projected rotation about the Eurasian-Marmara block pole (located 36.9°N, 28.6°E [*Meade et al.*, 2002]). Fault slip is induced by moving the northern (Eurasian) model edge at a 23 mm/yr rate [*Meade et al.*, 2002; *Le Pichon et al.*, 2003]. The southern model edge is held fixed to the Marmara block, and is not free to move laterally. The model base is freely slipping laterally, but cannot move vertically.

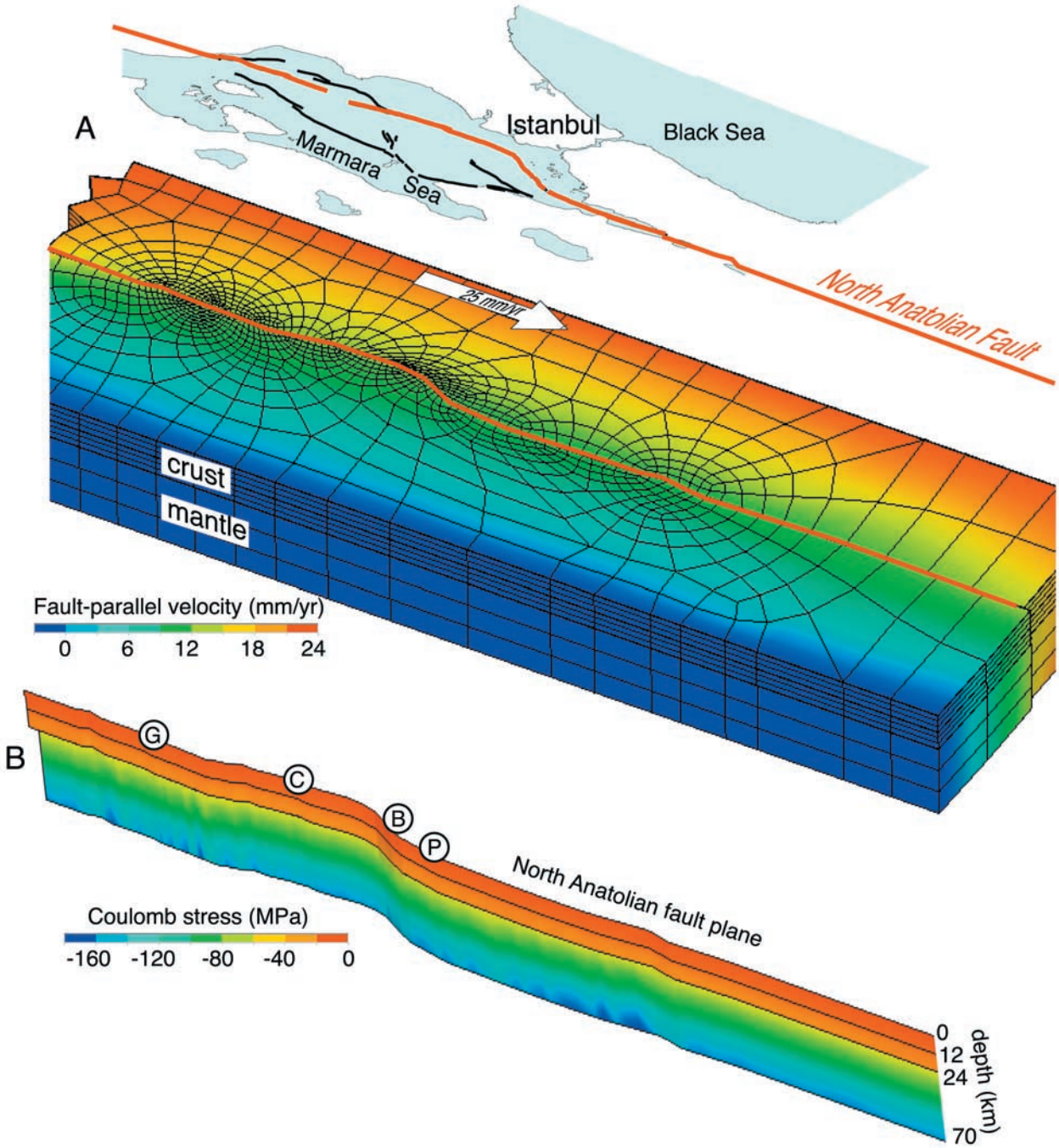

Figure 11. Finite element model of the Sea of Marmara lithosphere used to determine tectonic stressing rates along the North Anatolian fault. The north edge of the model is the horizontal projection of the relative motion about the pole of rotation between the Marmara block and Eurasia [*Meade et al.*, 2002]. The seismogenic part of the modeled North Anatolian fault is kept locked, and the relative plate motion (23 mm/yr) is imposed along the north model edge. The rate of Coulomb stress growth on the locked fault is then tracked over time. The labels G, C, P, and B correspond to points on the model North Anatolian fault where Coulomb-stress-versus-time plots (shown in Figure 13) were made.

[47] The model is composed entirely of eight-node viscoelastic elements. The proportion of viscous to elastic behavior of a given element node is governed by the local crustal geotherm derived from heat flow measurements [*Pfister et al.*, 1998]. Temperature dependence of strain rate ($\dot{\varepsilon}$) in the model is controlled by the creep equation

$$\dot{\varepsilon} = A \exp(-Q_c/RT)\sigma^n \qquad (10)$$

[e.g., *Kirby and Kronenberg*, 1987], where A, Q_c (activation energy), and n are experimentally derived elastic constants, R is the universal gas constant, T is temperature, and σ is differential stress. In the lower-temperature upper crust, the model behaves elastically, while deeper, higher-temperature regions behave increasingly more viscoelastically.

[48] The finite element model has a cut through the crust [e.g., *Parsons*, 1998; *Bürgmann et al.*, 2002] that represents the North Anatolian fault in the Marmara Sea region; it is modeled as throughgoing [*Le Pichon et al.*, 2001], though in reality the fault may be interrupted by a step over in the central Sea of Marmara (Figure 3) [*Armijo et al.*, 2002]. This issue is unimportant for the stressing rate calculation because the model fault is locked throughout the upper crust. The modeled fault is deformable, and is constructed from contact elements that obey the Coulomb failure relation. Contact elements have zero thickness and are welded to the sides of viscoelastic elements. The Eurasian plate was moved past the Marmara block at a 23 mm/yr rate with the upper crustal faults locked so that the rate of Coulomb stress accumulation on the faults could be determined. When the seismogenic (0–12.5 km) parts of the faults are locked, the finite element model can roughly reproduce the transitional surface deformation rates measured across the North Anatolian fault zone with GPS [*Reilinger et al.*, 2000] (Figure 12). For the crustal stressing rates to be valid, the strain rates must be matched.

4.2.2. Stressing Rate Calculations

[49] The modeled rate of Coulomb stress accumulation on the North Anatolian fault in the Sea of Marmara depends mostly on the orientation of the fault with respect to the relative plate motion vector. The highest calculated rate is on the Ganos segment (0.0064 MPa/yr), which most closely parallels the relative motion direction (Figures 1 and 13). The lowest calculated stressing rate (0.001 MPa/yr) is on the sharp releasing bend of the Prince's Islands segment (Figures 1 and 13). It may thus require significant stress concentration on the fault on either side of the releasing bend to propagate an earthquake through the bend; the A.D. 1500–2000 catalog suggests that this has happened in 1509 and again in 1766 (Figure 3).

[50] Calculations were also made for the differential stressing rate in the Çinarcik basin, which is a suggested location for the 2 September 1754 and 10 July 1894 $M \sim 7.0$ earthquakes. The dip of the mapped normal faults in the basin is not known, so the differential stressing rate in the basin crust is calculated assuming that the faults are optimally oriented. For this calculation the strike-slip faults are allowed to slip, since extensional stress in the Çinarcik basin is likely a result of the releasing orientation of the North Anatolian fault with respect to the relative plate motion vector [e.g., *Armijo et al.*, 1999; *Le Pichon et al.*, 2003]. The differential stressing rate in and around the basin is ~0.05 MPa/yr, with the least principal stress oriented nearly orthogonal to the strike of the North Anatolian fault (Figure 14). That orientation is also orthogonal to the mapped normal faults as would be expected.

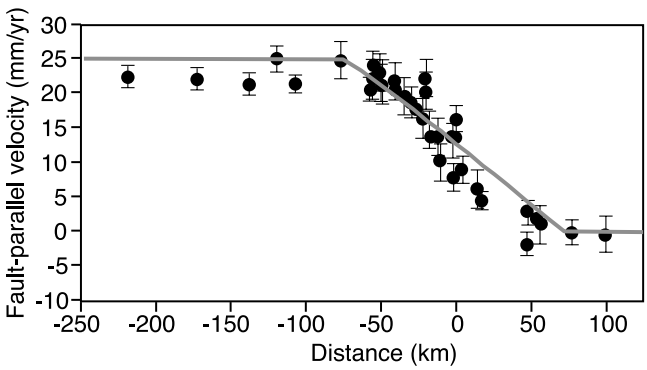

Figure 12. Comparison between surface velocity relative to the Marmara block in the finite element model (solid line) and GPS observations [*Reilinger et al.*, 2000] across the North Anatolian fault zone.

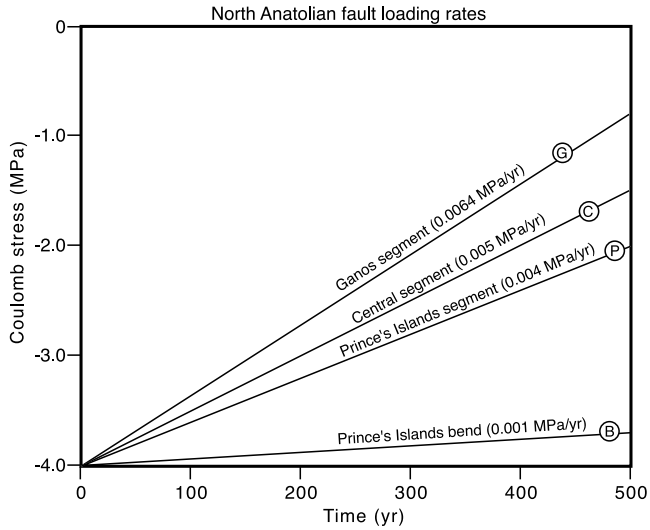

Figure 13. Coulomb stressing rate at various points along the modeled North Anatolian fault. The curves labeled G, C, P, and B are calculated at the locations with the same labels in Figure 10.

4.3. Interaction Probability Calculations

[51] All of the necessary parameters have been assembled to make interaction probability calculations for the faults submerged beneath the Sea of Marmara. Interevent and elapsed time values were gathered/modeled from the A.D. 1500–2000 earthquake catalog. There is no consensus on an appropriate aperiodicity value, so all calculations are made using $\alpha = 0.2$ and $\alpha = 0.5$, which in combination with the Poisson probability calculations, encompasses the full range of possibilities [e.g., *WGCEP*, 2003]. The change in stress caused by the Izmit earthquake was modeled from elastic dislocation calculations made from three coseismic slip distributions, and one afterslip model. The aftershock duration was determined empirically, and from that and the modeled tectonic stressing rates, the combination of normal stress and constitutive constant $A\sigma$, was calculated.

[52] Reported interaction probability values are the means of 1000 calculations with parameters drawn at random from Brownian-distributed interevent times (with aperiodicity (α) either 0.2 or 0.5), and the other parameters drawn from normal distributions about their mean values. Stress changes

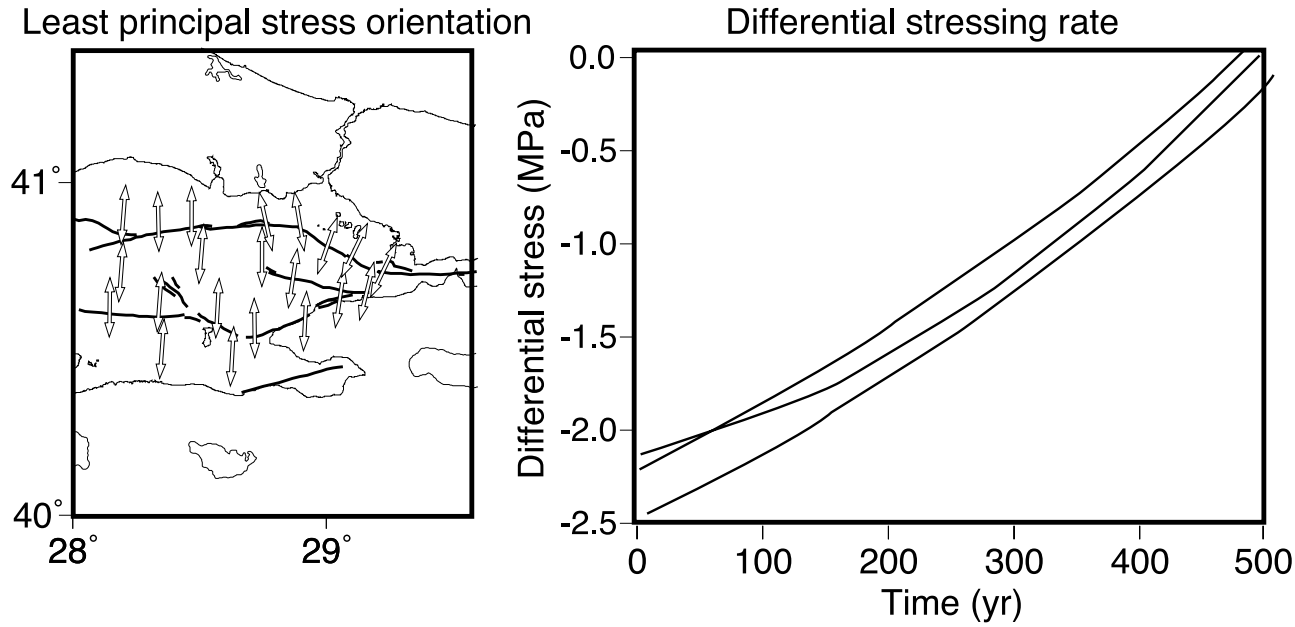

Figure 14. Least principal stress orientations and differential stressing rates in and around the extensional Çinarcik basin. Calculated least stress orientations tend to be perpendicular to mapped normal faults in the basin.

were drawn at random from a normal distribution with coefficient of variation (COV) of 0.35 (section 3.2), where the COV is defined as the standard deviation divided by the distribution mean. The COV is a shape parameter appropriate for a normal distribution, and is analogous to the aperiodicity (α) of the Brownian distribution. The aftershock duration and loading rate were drawn from normal distributions with COV = 0.25 after *Parsons et al.* [2000]. The purpose for these Monte Carlo calculations is to investigate the sensitivity of the probability values to variations in the input parameters [*Savage*, 1991, 1992]. Thus the ranges in values are not formal uncertainties, which do not have any meaning when associated with a probability which is itself an expression of uncertainty. The sensitivity of the probability values is a useful measure of the potential range of the hazard under given assumptions, and of the relative importance of different aspects of the problem such as the historical earthquake catalog and the influence of stress transfer and earthquake interactions.

[53] Interaction probability calculations are made for two North Anatolian fault segments, the Prince's Islands and Ganos, and on the floating $M \sim 7.0$ sources in the Çinarcik basin. Quoted sensitivities on reported probabilities are one standard deviation (1σ) on the Monte Carlo calculations. The Prince's Islands segment is affected most by the Izmit earthquake; the 2004–2034 probability of a M $\geq$ 7 earthquake rises from an 11% Poisson probability to 22 ± 12% if $\alpha = 0.5$, and 36 ± 24% if $\alpha = 0.2$ when time dependence is introduced, and rises to 31 ± 15% if $\alpha = 0.5$, and to 54 ± 26% if $\alpha = 0.2$ when coseismic stress changes are included. If the afterslip stress change model is used, the 30 year Prince's Islands segment probability rises to 34 ± 14% if $\alpha = 0.5$, and 62 ± 25% if $\alpha = 0.2$. The Ganos segment and normal faults in the Çinarcik basin are calculated to have been negligibly affected by the Izmit earthquake and afterslip, with a probability change of <1% (Table 3).

[54] An earthquake on the Prince's Islands segment of the North Anatolian fault or in the Çinarcik basin would shake Istanbul more strongly than an equivalent event on the other identified segments (Figure 1). Thus the probability of failure on the Prince's Islands segment along with the floating $M \geq 7$ sources reasonably estimate the odds of strong shaking (MMI $\geq$ VIII [*Parsons et al.*, 2000]) in the city. Therefore the 30 year interaction probability at Istanbul is 41 ± 14% if $\alpha = 0.5$ and 66 ± 25% if $\alpha = 0.2$. *Parsons et al.* [2000] calculated a 62 ± 15% probability for Istanbul using $\alpha = 0.5$ because three sources of MMI $\geq$ VIII shaking were identified using an older fault map and associated A.D. 1500–2000 catalog.

4.4. Are Time-Dependent and Interaction Probability Changes Significant?

[55] Monte Carlo exploration of parameter ranges in time-dependent and interaction probability calculations highlights some difficulties in making a probabilistic earthquake forecast. Uncertainty of earthquake recurrence dominates the variability of probability calculations, even if the aperiodicity on interevent time is 0.2 (Table 3). The lower ends of the 1σ sensitivity ranges in all the time-dependent calculations nearly encompass the Poisson calculations, suggesting that for a region as large as the Sea of Marmara, one end-member of the time-dependent model is earthquakes occurring randomly in time. Similarly, stress increases calculated from coseismic and postseismic Izmit earthquake slip do not raise time-dependent probability beyond the high end of the 1σ parameter sensitivities (Table 3). Strictly speaking then, neither the introduction of time dependence nor interaction alone produces significant probability changes. Additionally, interaction and time dependence together do not alter the combined Sea of Marmara regional earthquake probability beyond the 1σ parameter sensitivities from the combined regional Poisson

probability (Table 3). However, a combination of stress interactions and time dependence can alter individual fault segments significantly from the Poisson values; compare the interaction probability of 31–54% for the Prince's Islands fault with the Poisson value of 11%. Thus time-dependent interaction probability methods might best be used as a means of assessing the relative probability amongst a group of fault segments rather than to make aggregate calculations on a regional scale.

[56] In summary, the concepts of time dependence and stress transfer appear to be useful tools in assessing the likely order of future earthquakes in a region, and to compare the hazard at different locations. For example, the time-dependent interaction probability values for the Sea of Marmara region are not very different from a simple Poission model (compare 53 ± 18% with 38%). However, the values in the eastern Sea of Marmara at Istanbul are much different at 41 ± 14% (interaction; $\alpha = 0.5$) versus 21% (Poisson). It is concluded that two factors give the time-dependent interaction values significance for Istanbul: (1) incorporation of the long elapsed time since the last large earthquake on the Prince's Islands fault (238 years since 1766) in the time-dependent calculation, and (2) the largest calculated stress increases from the 1999 Izmit earthquake occur on the Prince's Islands fault maximizing the interaction effect relative to other Sea of Marmara faults.

5. Conclusions

[57] The probability of a $M \geq 7$ earthquake rupturing beneath the Sea of Marmara is ~35–70% in the next 30 years if a time-dependent model that includes coseismic and postseismic effects of the 1999 $M = 7.4$ Izmit earthquake is used. Despite one of the world's longest written records of earthquake occurrence, uncertainties in the interevent model lead to the broad range of possible earthquake probability. Improved Marmara Sea fault mapping, a new earthquake attenuation relation, and a new regional relationship between M and surface slip enable a new A.D. 1500–2000 earthquake catalog calculated from damage descriptions that identifies four primary $M \geq 7$ earthquake sources (Figure 1): (1) the Izmit segment of the North Anatolian fault, (2) a fault in the east Sea of Marmara here called the Prince's Islands segment of the North Anatolian fault, (3) a segment in the west Sea of Marmara (west of the Central Basin step over (Figures 1 and 3)) that emerges on land as the Ganos segment of the North Anatolian fault, and (4) normal faults in the Çinarcik basin and southern Sea of Marmara. The A.D. 1500–2000 earthquake catalog indicates two events on each of the North Anatolian segments, and three events in the Çinarcik basin/southern Sea of Marmara. Using the new catalog to calculate time-dependent probability without any interaction effects yields a ~44 ± 18% probability of a $M \geq 7$ earthquake somewhere in the region over the next 30 years. This value is nearly the same as the regional combined Poisson probability of ~38%, except that under the time-dependent model, most of the regional probability shifts to the Prince's Islands fault in the eastern Sea of Marmara near Istanbul.

[58] More detailed coseismic and postseismic slip models of the 1999 $M = 7.4$ Izmit earthquake combined with better Marmara Sea fault mapping allow presumably more accurate stress transfer calculations, which add a mean 7–16% probability increase above background depending on parameter choices. Monte Carlo exploration of parameters shows that uncertainty in interevent times (COV ranges from 0.2 to 0.5) has by far the greatest impact on probability values (Table 3). Thus input parameter variability exceeds the impact of stress interactions on the regional calculations. However, it is concluded that valuable information is conveyed by reporting the mean interaction probability and the 1σ parameter sensitivity range because individual fault segment probabilities can be affected more than the 1σ parameter sensitivity range. For example, the Prince's Islands fault probability, already increased by time dependence, is further increased by the largest stress transfer effect of the Izmit shock. These combined effects cause the probability of MMI≥VIII shaking in Istanbul over the 2004–2034 interval to rise from a Poisson estimate of 21% to values of 41 ± 14% ($\alpha = 0.5$) and 66 ± 25% ($\alpha = 0.2$) under the time-dependent interaction model.

Appendix A: A.D. 1500–2000 Earthquake Catalog Events

A1. The 10 September 1509 Earthquake

[59] One of the largest and most damaging earthquakes to strike the eastern Mediterranean region, this event was extremely destructive in Istanbul, was felt as far away as the Danube region, Greece, and the Nile delta, and caused an eastern Marmara Sea tsunami [*Ambraseys and Finkel*, 1990, 1995]. *Parsons et al.* [2000] located this earthquake in the southern Marmara Sea (Figure 2) because no fault model indicated any other segment of sufficient length to accommodate the $M \sim 7.4$ quake. The new fault model of *Armijo et al.* [2002] indicates less continuity in the southern Sea of Marmara and more on the main trace of the North Anatolian fault. Following the rules set out in section 2.1, I thus relocate this earthquake to the main trace of the North Anatolian fault with a western bound at the Central basin step over, and an eastern boundary near the Hersek Peninsula. *Ambraseys* [2002] located this event epicenter in the Sea of Marmara near Istanbul, and calculated its size as $M_s = 7.2$.

A2. The 10 May 1556 Earthquake

[60] A destructive earthquake was felt around the Sea of Marmara with damage reported at Edincik, Bursa and Istanbul [*Ambraseys and Finkel*, 1995]. The limited distribution of damage reports and omission of descriptions in many areas makes this earthquake very difficult to locate with any confidence. It was assigned a $M_s = 7.1$ by *Ambraseys* [2002], who suggested that it ruptured a fault beneath the southern Sea of Marmara, or the southern strand of the North Anatolian fault south of the Sea of Marmara. In either case this earthquake is not included in the interevent model because if it did occur beneath the southern Sea of Marmara, it is the only large quake to do so in that location during the past ~2000 years [*Ambraseys*, 2002] (Figure 1).

A3. The 25 May 1719 Earthquake

[61] A major earthquake shook the eastern Sea of Marmara, and was especially damaging in the Gulf of Izmit, destroying many of the towns and cities along the coast

there; significant damage was also reported in Istanbul [*Ambraseys and Finkel*, 1991, 1995]. This $M \sim 7.4$ rupture is best fit to the MMI values if it is located in the Gulf of Izmit and east of the Sea of Marmara (Figure 3), roughly the same part of the North Anatolian fault that slipped during the 1999 M = 7.4 Izmit earthquake. *Ambraseys* [2002] cataloged this event as M_s = 7.4, located ~15 km west of Izmit.

A4. The 2 September 1754 Earthquake

[62] Another large earthquake struck in the eastern Sea of Marmara just over 35 years after the 1719 event (though less severe), with most damage recorded in Istanbul; it was associated with a small tsunami [*Ambraseys and Finkel*, 1991, 1995]. The relatively sparse MMI interpretations from damage descriptions permit two possible segment ruptures for this $M \sim 7.0$ event: (1) in the Çinarcik basin where there are mapped normal faults of sufficient length (Figure 3) probably related to the releasing bend of the North Anatolian fault near the Prince's Islands (Figure 3), or (2) the 1754 event filled an unruptured gap on the North Anatolian fault between the 1719 and May 1766 shocks. *Ambraseys* [2002] placed this earthquake along the northern Çinarcik basin and calculated M_s = 6.8.

A5. The 22 May 1766 Earthquake

[63] This earthquake was destructive in Istanbul, but caused more damage to the west in Thrace than did the 1754 event; it was also associated with a damaging tsunami in the Bosphorus [*Ambraseys and Finkel*, 1991, 1995]. The only fault segment of sufficient length to accommodate this $M \sim 7.2$ shock that can satisfy the MMI distribution, appears to be the main trace of the North Anatolian fault (Figure 3). The damage distribution is similar to the $M \sim 7.4$ 1509 earthquake (Figure 3), and the May 1766 event probably ruptured much of the same fault segment as slipped in 1509. *Ambraseys* [2002] calculated M_s = 7.1 and placed it on the North Anatolian fault slightly west of the 1754 earthquake, adjacent to Istanbul.

A6. The 5 August 1766 Earthquake

[64] This large earthquake most affected the western Sea of Marmara, in the Ganos region, and was more severe than the May 1766 quake to the east [*Ambraseys and Finkel*, 1991, 1995]. The best fit to the MMI interpretations from damage descriptions is a $M \sim 7.6$ rupture of the North Anatolian fault east of the Central basin step over, and toward the west along the Gallipoli Peninsula (Figure 3). A trenching study found evidence for this earthquake near Kavakkoy, where the North Anatolian fault enters the Gulf of Saros [*Rockwell*, 2000]. *Ambraseys* [2002] calculated M_s = 7.4 and also located it on the Gallipoli Peninsula.

A7. The 10 July 1894 Earthquake

[65] This earthquake was destructive in the Gulf of Izmit, but also damaged Istanbul; the main shock caused a tsunami with a 1.5 m height [*Ambraseys and Finkel*, 1991; *Ambraseys*, 2001]. Calculations from MMI values place the likely rupture of this $M \sim 7.0$ event either on the north or south edge of the Çinarcik basin (Figure 3). *Ambraseys* [2001] concluded from the distribution of damage that the 1894 event occurred in the Gulf of Izmit, and may have overlapped the 1999 Izmit rupture; a trenching study near Izmit also suggested overlap with the 1999 event [*Tsutsumi et al.*, 2002]. *Le Pichon et al.* [2003] suggested this event may have occurred on a normal fault. Generation of a tsunami requires some vertical seafloor motion and might favor a normal fault origin along the southern Çinarcik basin except that earthquakes interpreted to have ruptured the Prince's Islands releasing bend (1509; May 1766) were also tsunamigenic. Thus like the 1754 earthquake, there are two possible fault sources for this earthquake.

A8. The 13 September 1912 Earthquake

[66] This M_s = 7.4 earthquake struck the Gallipoli Peninsula region, destroying more than 300 villages; the on land part of the rupture was associated with a 50-km-long fault break [*Ambraseys and Finkel*, 1991]. The 360 MMI observations from this earthquake were used to test the magnitude location determination methods as discussed previously.

A9. The 17 August 1999 Earthquake

[67] The M = 7.4 Izmit earthquake ruptured the North Anatolian fault from the western Gulf of Izmit to the town of Gölyaka in the east; the on land fault break was 145 km long [*Barka et al.*, 2002]. This event killed more than 18,000 people and collapsed, or heavily damaged about 75,000 buildings.

Appendix B: Rate-State Transient Probability Change

[68] *Dieterich* [1994] derived a time-dependent seismicity rate $R(t)$, after a stress perturbation as

$$R(t) = \frac{r}{\left[\exp\left(\frac{-\Delta t}{a s}\right) - 1\right] \exp\left[\frac{-t}{t_a}\right] + 1}, \tag{B1}$$

where r is the steady state seismicity rate, $\Delta\tau$ is the stress step, σ is the normal stress, a is a fault constitutive constant, and t_a is an observed aftershock duration, a fault-specific parameter. An example application of this concept is to earthquake clustering and aftershocks, where $R(t)$ takes the form of Omori's law.

[69] The transient change in expected earthquake rate $R(t)$ after a stress step can be related to the probability of an earthquake of a given size over the time interval Δt through a nonstationary Poisson process as

$$P(t, \Delta t) = 1 - \exp\left[-\int_t^{t+\Delta t} R(t)dt\right] = 1 - \exp(-N(t)), \tag{B2}$$

after *Dieterich and Kilgore* [1996], where $N(t)$ is the expected number of earthquakes in the interval Δt. This transient probability change is superimposed on the permanent change that results from a time shift, or a change in the repeat time as discussed previously. Integrating for $N(t)$ yields

$$N(t) = r_p \left\{ \Delta t + t_a \ln \left[\frac{1 + \left[\exp\left(\frac{-\Delta\tau}{a\sigma}\right) - 1\right] \exp\left[\frac{-\Delta t}{t_a}\right]}{\exp\left(\frac{-\Delta\tau}{a\sigma}\right)} \right] \right\}, \tag{B3}$$

where r_p is the expected rate of earthquakes associated with the permanent probability change [*Toda et al.*, 1998]. This rate can be determined by again applying a stationary Poisson probability expression as

$$r_p = \left(\frac{-1}{\Delta t}\right) \ln(1 - P_c), \tag{B4}$$

where P_c is a conditional probability, and can be calculated using any distribution. The Brownian Passage Time model is used here [*Matthews et al.*, 2002] (equation (7)).

[70] **Acknowledgments.** I thank Michel Bouchon, Roland Bürgmann, Bertrand De Louis, Xu Li, and Haruko Sekiguchi for sharing their Izmit earthquake source models. Many of the ideas presented in this paper were developed with a working group that included Bill Bakun, Aykut Barka, Jim Dieterich, Ross Stein, and Shinji Toda. Substantial improvements were made as a result of insightful reviews by Massimo Cocco, Rodolfo Console, Joan Gomberg, Ross Stein, and Shinji Toda. Partial funding from SwissRe is gratefully acknowledged.

References

Aki, K. (1965), Maximum likelihood estimate of b in the formula log N = *a*–*b*M and its confidence limits, *Bull. Earthquake Res. Inst.*, *43*, 237–239.

Ambraseys, N. N. (1988), Engineering seismology, *Earthquake Eng. Struct. Dyn.*, *17*, 1–105.

Ambraseys, N. N. (2001), The earthquake of 10 July 1894 in the Gulf of Izmit (Turkey) and its relation to the earthquake of 17 August 1999, *J. Seismol.*, *5*, 117–128.

Ambraseys, N. N. (2002), The seismic activity of the Marmara Sea region over the last 2000 years, *Bull. Seismol. Soc. Am.*, *92*, 1–18.

Ambraseys, N. N., and C. F. Finkel (1987), Seismicity of Turkey and neighboring regions, 1899–1915, *Ann. Geophys.*, *5*, 701–725.

Ambraseys, N. N., and C. F. Finkel (1990), The Marmara Sea earthquake of 1509, *Terra Nova*, *2*, 167–174.

Ambraseys, N. N., and C. F. Finkel (1991), Long-term seismicity of Istanbul and the Marmara sea region, *Terra Nova*, *3*, 527–539.

Ambraseys, N. N., and C. F. Finkel (1995), *The Seismicity of Turkey and Adjacent Areas: A Historical Review,1500–1800*, 240 pp., Muhittin Salih EREN, Istanbul.

Armijo, R., B. Meyer, A. Hubert, and A. Barka (1999), Westward propagation of the North Anatolian fault into the northern Aegean: Timing and kinematics, *Geology*, *27*, 267–270.

Armijo, R., B. Meyer, S. Navarro, G. King, and A. Barka (2002), Asymmetric slip partitioning in the Sea of Marmara pull-apart: A clue to propagation processes of the North Anatolian fault?, *Terra Nova*, *14*, 80–86.

Bakun, W. H., and C. M. Wentworth (1997), Estimating earthquake location and magnitude from seismic intensity data, *Bull. Seismol. Soc. Am.*, *87*, 1502–1521.

Barka, A. A. (1996), Slip distribution along the North Anatolian fault associated with large earthquakes of the period 1939 to 1967, *Bull. Seismol. Soc. Am.*, *86*, 1234–1238.

Barka, A. A., et al. (2002), The surface rupture and slip distribution of the 17 August 1999 Izmit earthquake (M 7.4), North Anatolian Fault, *Bull. Seismol. Soc. Am.*, *92*, 43–60.

Bouchon, M., M. N. Toksoz, H. Karabulut, M.-P. Bouin, M. Dietrich, M. Aktar, and M. Edie (2002), Space and time evolution of rupture and faulting during the 1999 Izmit (Turkey) earthquake, *Bull. Seismol. Soc. Am.*, *92*, 256–266.

Bürgmann, R., S. Ergintav, P. Segall, E. H. Hearn, S. C. McClusky, R. E. Reilinger, H. Woith, and J. Zschau (2002), Time-dependent distributed afterslip on and deep below the Izmit earthquake rupture, *Bull. Seismol. Soc. Am.*, *92*, 1450–1469.

Caristan, Y. (1982), The transition from high temperature creep to fracture in Maryland diabase, *J. Geophys. Res.*, *87*, 6781–6790.

Carter, N. L., and M. C. Tsenn (1987), Flow properties of the lithosphere, *Tectonophysics*, *136*, 27–63.

De Louis, B., D. Giardini, P. Lundgren, and J. Salichon (2002), Joint inversion of InSAR, GPS, teleseismic, and strong-motion data for the spatial and temporal distribution of earthquake slip: Application to the 1999 Izmit mainshock, *Bull. Seismol. Soc. Am.*, *92*, 278–299.

Dieterich, J. H. (1994), A constitutive law for rate of earthquake production and its application to earthquake clustering, *J. Geophys. Res.*, *99*, 2601–2618.

Dieterich, J. H., and B. Kilgore (1996), Implications of fault constitutive properties for earthquake prediction, *Proc. Natl. Acad. Sci. USA*, *93*, 3787–3794.

Dutton, C. E. (1904), *Earthquakes in the Light of the New Seismology*, 314 pp., G. P. Putnam, New York.

Felzer, K. R., R. E. Abercrombie, and G. Ekström (2003), Secondary aftershocks and their importance for aftershock forecasting, *Bull. Seismol. Soc. Am.*, *93*, 1433–1448.

Hagiwara, Y. (1974), Probability of earthquake occurrence as obtained from a Weibull distribution analysis of crustal strain, *Tectonophysics*, *23*, 313–318.

Hansen, F. D., and N. L. Carter (1983), Semibrittle creep of dry and wet Westerly granite at 1000 MPa, in *24th U.S. Symposium on Rock Mechanics*, pp. 429–447, Tex. A&M Univ., College Station.

Harris, R. A. (1998), Introduction to special section: Stress triggers, stress shadows, and implications for seismic hazard, *J. Geophys. Res.*, *103*, 24,347–24,358.

Hearn, E. H., R. Bürgmann, and R. E. Reilinger (2002), Dynamics of Izmit earthquake postseismic deformation and loading of the Düzce earthquake hypocenter, *Bull. Seismol. Soc. Am.*, *92*, 172–193.

Horasan, G., L. Gülen, A. Pinar, D. Kalafat, N. Özel, H. S. Kuleli, and A. M. Isikara (2002), Lithospheric structure of the Marmara and Aegean regions, western Turkey, *Bull. Seismol. Soc. Am.*, *92*, 322–329.

Hubert-Ferrari, A., A. Barka, E. Jaques, S. S. Nalbant, B. Meyer, R. Armijo, P. Tapponnier, and G. C. P. King (2000), Seismic hazard in the Marmara Sea region following the 17 August 1999 Izmit earthquake, *Nature*, *404*, 269–273.

Ito, A., et al. (1999), Precise distribution of aftershocks of the Izmit earthquake of August 17, 1999, Turkey, *Eos Trans. AGU*, *80*(46), Fall Meet. Suppl., F662.

Jackson, J. (2002), Strength of the continental lithosphere: Time to abandon the jelly sandwich?, *GSA Today*, *12*, 4–9.

Kagan, Y. Y. (1994), Incremental stress and earthquakes, *Geophys. J. Int.*, *117*, 345–364.

Kagan, Y. Y., and D. D. Jackson (1991), Long-term earthquake clustering, *Geophys. J. Int.*, *104*, 117–133.

Ketin, I. (1969), Uber die nordanatolische Horizontalverschiebung, *Bull. Min. Res. Explor. Inst. Turkey*, *72*, 1–28.

Kilb, D., J. Gomberg, and P. Bodin (2002), Aftershock triggering by complete Coulomb stress changes, *J. Geophys. Res.*, *107*(B4), 2060, doi:10.1029/2001JB000202.

Kirby, S. H., and A. K. Kronenberg (1987), Rheology of the lithosphere: Selected topics, *Rev. Geophys.*, *25*, 1219–1244.

Lachenbruch, A. H., and P. Morgan (1990), Continental extension, magmatism, and elevation: Formal relations and rules of thumb, *Tectonophysics*, *174*, 39–62.

Le Pichon, X., et al. (2001), The active main Marmara Fault, *Earth Planet. Sci. Lett.*, *192*, 595–616.

Le Pichon, X., N. Chamot-Rooke, C. Rangin, and A. M. C. Sengör (2003), The North Anatolian fault in the Sea of Marmara, *J. Geophys. Res.*, *108*(B4), 2179, doi:10.1029/2002JB001862.

Li, X., V. F. Cormier, and M. N. Toksoz (2002), Complex source process of the 17 August 1999 Izmit, Turkey, earthquake, *Bull. Seismol. Soc. Am.*, *92*, 267–277.

Lindh, A. G. (2004), Long-term earthquake forecasts in the San Francisco Bay area, *Bull. Seismol. Soc. Am*, in press.

Marcellini, A. (1997), Physical model of aftershock temporal behavior, *Tectonophysics*, *277*, 137–146.

Matthews, M. V., W. L. Ellsworth, and P. A. Reasenberg (2002), A Brownian model for recurrent earthquakes, *Bull. Seismol. Soc. Am.*, *92*, 2233–2250.

McClusky, S., et al. (2000), Global Positioning System constraints on plate kinematics and dynamics in the eastern Mediterranean and Caucasus, *J. Geophys. Res.*, *105*, 5695–5719.

Meade, B. J., B. H. Hager, S. C. McClusky, R. E. Reilinger, S. Ergintav, O. Lenk, A. Barka, and H. Özener (2002), Estimates of seismic potential in the Marmara Sea region from block models of secular deformation constrained by Global Positioning System measurements, *Bull. Seismol. Soc. Am.*, *92*, 208–215.

Nakamura, A., A. Hasegawa, A. Ito, B. Üçer, S. Baris, Y. Honkura, T. Kono, S. Hori, R. Pektas, T. Kolmut, C. Çelik, and A. M. Isikara (2002), P-wave velocity of the crust and its relationship to the occurrence of the 1999 Izmit, Turkey, earthquake and aftershocks, *Bull. Seismol. Soc. Am.*, *92*, 330–338.

Nalbant, S. S., A. Hubert, and G. C. P. King (1998), Stress coupling between earthquakes in northwest Turkey and the north Aegean Sea, *J. Geophys. Res.*, *103*, 24,469–24,486.

Nishenko, S. P., and R. Buland (1987), A generic recurrence interval distribution for earthquake forecasting, *Bull. Seismol. Soc. Am.*, *77*, 1382–1399.

Ogata, Y. (1999), Estimating the hazard of rupture using uncertain occurrence times of paleoearthquakes, *J. Geophys. Res.*, *104*, 17,995–18,014.
Okada, Y. (1992), Internal deformation due to shear and tensile faults in a half-space, *Bull. Seismol. Soc. Am.*, *82*, 1018–1040.
Omori, F. (1894), On aftershocks, *Rep. Imp. Earthquake Invest. Comm.*, *2*, 103–109.
Öncel, A. O., and M. Wyss (2000), The major asperities of the 1999 M_w = 7.4 Izmit earthquake defined by the microseismicity of the two decades before it, *Geophys. J. Int.*, *143*, 501–506.
Parke, J. R., T. A. Minshull, G. Anderson, R. S. White, D. McKenzie, I. Kuscu, J. M. Bull, N. Gorur, and C. Sengor (1999), Active faults in the Sea of Marmara, western Turkey, imaged by seismic reflection profiles, *Terra Nova*, *11*, 223–227.
Parsons, T. (1998), Seismic-reflection evidence that the Hayward fault extends into the lower crust of the San Francisco Bay area, California, *Bull. Seismol. Soc. Am.*, *88*, 1212–1223.
Parsons, T. (2002a), Global Omori law decay of triggered earthquakes: Large aftershocks outside the classical aftershock zone, *J. Geophys. Res.*, *107*(B9), 2199, doi:10.1029/2001JB000646.
Parsons, T. (2002b), Post-1906 stress recovery of the San Andreas fault system from three-dimensional finite element analysis, *J. Geophys. Res.*, *107*(B8), 2162, doi:10.1029/2001JB001051.
Parsons, T., S. Toda, R. S. Stein, A. Barka, and J. H. Dieterich (2000), Heightened odds of large earthquakes near Istanbul: An interaction-based probability calculation, *Science*, *288*, 661–665.
Pfister, M., L. Rybach, and S. Simsek (1998), Geothermal reconnaissance of the Marmara Sea region (NW Turkey): Surface heat flow density in an area of active continental extension, *Tectonophysics*, *291*, 77–89.
Reilinger, R. E., et al. (2000), Coseismic and postseismic fault slip for the 17 August 1999, M = 7.5, Izmit, Turkey earthquake, *Science*, *289*, 1519–1524.
Rockwell, T. (2000), Paleoearthquake history of the North Anatolian fault, western Turkey: An investigation into the nature of earthquake recurrence as revealed by precise stratigraphic and historical records, San Diego, CA, in *Geological Sciences*, 28 pp., San Diego State Univ., San Diego, Calif.
Savage, J. C. (1991), Criticism of some forecasts of the National Earthquake Prediction Evaluation Council, *Bull. Seismol. Soc. Am.*, *81*, 862–881.
Savage, J. C. (1992), The uncertainty in earthquake conditional probabilities, *Geophys. Res. Lett.*, *19*, 709–712.
Scholz, C. H. (1968), Microfractures, aftershocks, and seismicity, *Bull. Seismol. Soc. Am.*, *58*, 1117–1130.
Stein, R. S. (1999), The role of stress transfer in earthquake occurrence, *Nature*, *402*, 605–609.
Stein, R. S., A. A. Barka, and J. H. Dieterich (1997), Progressive failure on the North Anatolian fault since 1939 by earthquake stress triggering, *Geophys. J. Int.*, *128*, 594–604.
Toda, S., R. S. Stein, P. A. Reasenberg, J. H. Dieterich, and A. Yoshida (1998), Stress transferred by the 1995 M_w = 6.9 Kobe, Japan, shock: Effect on aftershocks and future earthquake probabilities, *J. Geophys. Res.*, *103*, 24,543–24,565.
Toksoz, M. N., A. F. Shakal, and A. J. Michael (1979), Space-time migration of earthquakes along the North Anatolian fault zone and seismic gaps, *Pageoph*, *117*, 1258–1270.
Tsutsumi, H., S. Toda, O. Emre, M. Okuno, S. Ozalp, C. Yildirim, K. Takada, and T. Nakamura (2002), Recurrence of large earthquakes on the 1999 Izmit surface rupture, North Anatolian Fault, Turkey, *Eos Trans. AGU*, *83*(47), Fall Meet. Suppl., Abstract S11B-1152.
Wells, D. L., and K. J. Coppersmith (1994), New empirical relationships among magnitude, rupture length, rupture width, rupture area, and surface displacement, *Bull. Seismol. Soc. Am.*, *84*, 974–1002.
Working Group on California Earthquake Probabilities (WGCEP) (1990), Probabilities of large earthquakes in the San Francisco Bay region, California, *U.S. Geol. Surv. Circ.*, *1053*, 51 pp.
Working Group on California Earthquake Probabilities (WGCEP) (1999), Probabilities of large earthquakes in the San Francisco Bay region, California, *U.S. Geol. Surv. Open File Rep.*, *99-517*, 60 pp.
Working Group on California Earthquake Probabilities (WGCEP) (2003), Probabilities of large earthquakes in the San Francisco Bay region: 2002–2031, *U.S. Geol. Surv. Open File Rep.*, *03-214*, 235 pp.

T. Parsons, U.S. Geological Survey, Mail Stop 999, 345 Middlefield Road, Menlo Park, CA 94025, USA. (tparsons@usgs.gov)